

Half-hypermultiplets and incomplete/complete resolutions in F-theory

Naoto Kan,^a Shun'ya Mizoguchi,^{a,b} Taro Tani^c

^a*Graduate University for Advanced Studies (Sokendai)
Tsukuba, Ibaraki, 305-0801, Japan*

^b*Theory Center, Institute of Particle and Nuclear Studies, KEK
Tsukuba, Ibaraki, 305-0801, Japan*

^c*National Institute of Technology, Kurume College,
Kurume, Fukuoka, 830-8555, Japan*

E-mail: naotok@post.kek.jp, mizoguch@post.kek.jp, tani@kurume-nct.ac.jp

ABSTRACT: We consider resolutions of codimension-two enhanced singularities from $SO(12)$ to E_7 and from E_7 to E_8 in six-dimensional F-theory, where a half-hypermultiplet arises for generic complex structures achieving them. The exceptional fibers at the enhanced point exhibit different structures depending on how the colliding 7-brane approaches the stack of gauge 7-branes, as previously observed by Morrison and Taylor in the case of the enhancement from $SU(6)$ to E_6 . When the colliding brane approaches them as $O(s)$, where s is the coordinate of the base space along the gauge 7-branes, the resolution process ends up with fewer exceptional fibers than naively expected from the Kodaira classification, with a non-Dynkin intersection matrix including half-integral intersection numbers. We confirm that the exceptional fibers at the enhanced point form extremal rays of the cone of the positive weights of the relevant pseudo-real representation, explaining why a half-hypermultiplet arises there. By altering the ordering of the singularities blown up in the process, we obtain, for both $SO(12) \rightarrow E_7$ and $E_7 \rightarrow E_8$, the intersection diagram on every other row of the corresponding box graphs. We present detailed derivations of the intersection diagrams of the exceptional fibers at the singularity enhanced points by examining how an exceptional curve is lifted up on the chart arising due to the subsequent blowing-up process. When the colliding brane approaches the stack of branes as $O(s^2)$, we obtain additional conifold singularity at the enhanced point, which completes the full Dynkin diagram of the enhanced group as was found previously.

Contents

1	Introduction	2
2	Half-hypermultiplets in six-dimensional F-theory	4
3	$SO(12) \rightarrow E_7$	8
3.1	Incomplete resolution: Blowing up p_1 first	8
3.1.1	Blowing up process	8
3.1.2	Intersection patterns at $s \neq 0$ and $s = 0$	12
3.1.3	Intersection diagram at $s = 0$: Transmutation of a root into a weight	15
3.2	Complete resolution: Blowing up p_1 first	18
3.2.1	Blowing up process	18
3.2.2	Intersection diagram at $s = 0$	20
3.3	Incomplete resolution: Blowing up q_1 first	22
3.3.1	Blowing up process	22
3.3.2	Intersection diagram at $s = 0$: Differences from the p_1 -first case	24
3.4	Complete resolutions: Blowing up q_1 first	25
3.5	Other inequivalent orderings	26
3.6	Comparison with the results of the M-theory Coulomb branch analysis	29
4	$E_7 \rightarrow E_8$	30
4.1	Incomplete resolution: Blowing up p_2 first	30
4.1.1	Blowing up process	30
4.1.2	Intersection diagram at $s = 0$	34
4.2	Complete resolution	35
4.3	Incomplete/complete resolutions: Blowing up q_2 first	36
4.4	Other inequivalent orderings	39
5	Conclusions	41
A	Symplectic Majorana-Weyl spinors, pseudo-real representations and half-hypermultiplets	42
A.1	Symplectic Majorana-Weyl spinors	42
A.2	Pseudo-real representation and symplectic Majorana condition	43
A.3	$\frac{2\mathbf{n}}{2}$ hypermultiplets vs. $2\mathbf{n}$ $\frac{1}{2}$ hypermultiplets	44
A.4	Restriction on the complex scalars	45
B	Summary of $SU(6) \rightarrow E_6$	46
C	Small resolution of a conifold singularity	48

1 Introduction

The significance of F-theory [1] in modern particle physics model building cannot be overestimated. The characteristic features of the Standard Model can be naturally explained by the $SU(5)$ and $SO(10)$ grand unified theories, which are engineered in F-theory. It can achieve matter fields in the spinor representation as well as the exceptional group gauge symmetry. F-theory has an advantage over the $E_8 \times E_8$ heterotic string theory in that it can address the issue of the gauge/gravity coupling correlation in the latter [2]. F-theory can also generate up-type Yukawa couplings perturbatively forbidden in D-brane models [3, 4].

In F-theory, matter typically arises¹ at codimension-two singularities [5–9] in the base space of the elliptic fibration. To be specific, consider a six-dimensional F-theory compactified on an elliptically fibered three-fold defined by a hypersurface $\Phi(x, y, z, s) = 0$ in $\mathbb{C}^4 \ni (x, y, z, s)$ over a complex two-fold with local coordinates $(z, s) \in \mathbb{C}^2$. Over a generic point with fixed (z, s) , this equation describes a genus-one curve. We assume that this hypersurface has a codimension-one singularity of some compact group H along $z = 0$ for generic $s \neq 0$, which is enhanced to some compact group $G \supset H$ at a codimension-two particular locus along the line $z = 0$, say, at $s = 0$.

In this set-up, one typically obtains chiral matter hypermultiplets corresponding to the homogeneous Kähler manifold $G/(H \times U(1))$ [5–10] at the enhanced singularity. However, if G and H are such that

$$\begin{aligned} G &\supset H \times SU(2) \\ \dim G &= (\dim H, \mathbf{1}) \oplus (\mathbf{2n}, \mathbf{2}) \oplus (\mathbf{1}, \mathbf{3}), \end{aligned} \tag{1.1}$$

where $n = 10, 16, 28$ for $(G, H) = (E_6, SU(6)), (E_7, SO(12)), (E_8, E_7)$, respectively,² the matter arising there are not the full hypermultiplets but *half*-hypermultiplets for generic complex structures achieving such singularities.

In all the cases above, $\mathbf{2n}$ is a pseudo-real representation of H , of which the representation matrix can be written as an $Sp(2n)$ matrix. For these representations, one can impose the symplectic Majorana condition on the $2n$ complex spinors. One can also define a similar relation among $2n$ pairs of the complex scalars by using a $U(1)_R$ rotation. In this way, the degrees of freedom of hypermultiplets are halved, yielding half-hypermultiplets in these representations.

In [11], the resolution of a codimension-two enhancement from $SU(6)$ to E_6 was studied in six dimensions. It was shown there that, if the colliding brane approaches $z = 0$ like $O(s)$ which is the generic case, only *five* exceptional curves appear through the blowing-up process even at the singularity enhanced point. This type of resolution was called the *incomplete resolution* in [11]. Note that, by resolving a codimension-one E_6 singularity, one obtains *six* exceptional fibers consisting the IV^* fiber type of Kodaira.

¹aside from adjoint matter in four dimensions arising from 7-branes wrapped over a four-cycle with nontrivial relevant cohomologies.

²They are also the pairs (though different real forms) appearing in “magical” supergravity theories [12, 13].

This means that there are not enough new degrees of freedom arising at the enhanced point to generate matter in a full hypermultiplet. The five exceptional fibers form a curious non-Dynkin intersection diagram, however. In particular, some of the exceptional curves turn out to have self-intersection number $-\frac{3}{2}$. This is equal to the minus of the length squared of a *weight* of the **20** representation. One can verify that these five exceptional curves form extremal rays of the cone of the positive weights of the **20** representation. (Actually, one can show that there are just 20 integer linear combinations of these exceptional curves which have self-intersection number $-\frac{3}{2}$; half of them have positive coefficients and the other half have negative coefficients, giving a whole set of the weights of **20**.) Thus the matter forms a *single* **20** representation of $SU(6)$. This shows the mechanism of how the *half*-hypermultiplet appears in this codimension-two singularity enhancement. (Note that for a full hypermultiplet one needs two **20** representations, either one of which survives as massless matter in six dimensions.)

On the other hand, if the brane collides like $O(s^2)$, an extra singularity arises at the intersection. This is a conifold singularity. Resolving it yields another exceptional curve, completing the proper Dynkin intersection diagram expected from the ordinary Kodaira classification. This was called the *complete resolution* [11].

Higher codimension singularities were also studied in [14] by exploring the phases of three-dimensional gauge theory arising from the compactification of M-theory on a Calabi-Yau four-fold (see [15–18]). In this approach, the generation of a half-hypermultiplet was explained as a result of the reduction of the massless states occurring due to the monodromy among the fibers [14]. It was noted there that if the complex structure was tuned so that there were extra sections, the monodromy was reduced and a full hypermultiplet appeared.

In this paper, we study the resolutions of the other two cases, $SO(12) \rightarrow E_7$ and $E_7 \rightarrow E_8$, of the codimension-two singularity enhancement in which half-hypermultiplets appear as massless states at the singularity. The strategy is the same as that used in [11]. To blow up this singularity along the line $z = 0$ we replace the local ambient space \mathbb{C}^4 with

$$\widehat{\mathbb{C}}^4 = \{((x, y, z, s); (\xi : \eta : \zeta)) \in \mathbb{C}^4 \times \mathbb{P}^2 \mid x\eta - y\xi = y\zeta - z\eta = z\xi - x\zeta = 0\} \quad (1.2)$$

and consider the hypersurface in it. (1.2) inserts a continuous family of \mathbb{P}^2 along the complex line $z = 0$ for arbitrary $s \in \mathbb{C}$. Then we find that there still are several, (again) codimension-one singularities on the intersection of $\widehat{\mathbb{C}}^4$ (1.2) and the hypersurface $\Phi = 0$. To resolve these singularities, we further make a replacement similar to $\mathbb{C}^4 \rightarrow \widehat{\mathbb{C}}^4$ along each singular line and consider the hypersurface in this blown-up ambient space. Then if we still find some singularities of codimension one, we perform a codimension-one blow up along each of them. Repeating these steps we end up with either of the two cases:

- (1) The case where there are no more singularities of any kind on the final hypersurface.
- (2) The case where there are no more codimension-one singularities, but still there is an isolated codimension-two singularity at $s = 0$ on the final hypersurface.

This is the phenomenon known as the partial simultaneous resolution of singularities [14, 19–21], and which case we will end up with depends on the vanishing order of the relevant section of the projective-space bundle for the respective singularity enhancement. For the enhancement $SU(6) \rightarrow E_6$ studied in [11], the relevant section is the polynomial

$t_r(s)$ in eq.(2.6) (see below), for $SO(12) \rightarrow E_7$ it is $H_{n+4}(s)$, and for $E_7 \rightarrow E_8$ it is $f_{n+8}(s)$. We will show that, also for the cases $SO(12) \rightarrow E_7$ and $E_7 \rightarrow E_8$ we will consider in this paper, we are led to the result (1) if these sections vanish like $O(s)$ as $s \rightarrow 0$. The codimension-two singularity is then resolved only by the codimension-one blow-ups in the ambient space, and therefore the number of times of the blowing-up operations is the same as that needed to resolve a Kodaira H singularity for fixed generic $s \neq 0$. Thus there are not enough exceptional curves to form the proper Dynkin diagram of G as their intersection matrix. Even so, we will see that the intersection diagram of the exceptional curves obtained by the $s \rightarrow 0$ limit of the exceptional surfaces is different from the Dynkin diagram of H . Rather, it turns out that some of the curves have their self-intersection number $-\frac{3}{2}$, as was observed in [11] for the $SU(6) \rightarrow E_6$ enhancement.

We perform blowing-ups for all possible inequivalent orderings of blowing up the singularities in both the enhancements $SO(12) \rightarrow E_7$ and $E_7 \rightarrow E_8$. We find that the intersection diagram on *every other* row in Figures 33 and 44 of [14] can be obtained, but not all of them.³ Although the intersection diagrams are different, the fibers obtained in the limit $s \rightarrow 0$ always form extremal rays of the cone of the positive weights of the relevant pseudo-real representation.

On the other hand, if they vanish like $O(s^2)$, we are led to the result (2), where we need a further resolution of the isolated singularity. This is the complete resolution; we have one more additional node to the incomplete intersection diagram obtained in the incomplete resolution, obtaining the full Dynkin diagram of the group G . We will find that, as was observed in [11], this final singularity appearing at codimension two is a conifold singularity for all the cases we examine in this paper.

The plan of this paper is as follows. In section 2, we review in what circumstances massless matter fields appear as half-hypermultiplets in the global six-dimensional F-theory compactification on an elliptic Calabi-Yau three-fold over a Hirzebruch surface. In section 3, we present the detailed process of blow-ups for the codimension-two singularity enhancement from $SO(12)$ to E_7 . In section 4, we turn to the resolution of the enhancement from E_7 to E_8 . Section 5 summarizes the conclusions. In Appendix A, we explain the relations between symplectic Majorana-Weyl spinors, pseudo-real representations and half-hypermultiplets. In Appendix B, we summarize the results of [11] on the resolution of the enhancement $SU(6) \rightarrow E_6$. Finally, in Appendix C, we present a basic explanation of the small resolution of a conifold.

2 Half-hypermultiplets in six-dimensional F-theory

Half-hypermultiplets arise when the unbroken gauge group is $SU(6)$, $SO(12)$ or E_7 [7]. These models can be systematically obtained by tuning the complex structure of the $SU(5)$ model.

We start with the six-dimensional compactification on F-theory on an elliptically fibered Calabi-Yau three-fold over a Hirzebruch surface \mathbb{F}_n [5, 6]. Let z, z' be affine coordinates of

³In the enhancement $SU(6) \rightarrow E_6$ studied in [11], there is no such option since only one singularity appears at each step of blowing up.

the fiber and base \mathbb{P}^1 's, respectively. The Weierstrass model

$$y^2 = x^3 + f(z, z')x + g(z, z') \quad (2.1)$$

develops an $SU(5)$ singularity if [7]

$$\begin{aligned} f(z, z') &= -3h_{n+2}^4 + 12h_{n+2}^2 H_{n+4} z - 12(H_{n+4}^2 - h_{n+2} q_{n+6}) z^2 + f_{n+8} z^3 + f_8 z^4, \\ g(z, z') &= 2h_{n+2}^6 - 12h_{n+2}^4 H_{n+4} z + (24h_{n+2}^2 H_{n+4}^2 - 12h_{n+2}^3 q_{n+6}) z^2 \\ &\quad + (-f_{n+8} h_{n+2}^2 + 24h_{n+2} H_{n+4} q_{n+6} - 16H_{n+4}^3) z^3 \\ &\quad + (-f_8 h_{n+2}^2 + 2f_{n+8} H_{n+4} + 12q_{n+6}^2) z^4 + g_{n+12} z^5 + g_{12} z^6, \end{aligned} \quad (2.2)$$

where $h_{n+2}, H_{n+4}, q_{n+6}, f_{n+8}$ and g_{n+12} are polynomials of z' of degrees specified by the subscripts. They are sections of Looijenga's weighted projective space bundle [22–24] characterizing the $SU(5)_{\text{instanton}}$ vector bundle of the dual heterotic string theory. This Calabi-Yau three-fold admits a $K3$ fibration, and we work with one of the rational elliptic surfaces in the stable degeneration limit of the $K3$ so that the orders of the polynomials $f(z, z')$ and $g(z, z')$ are truncated at z^4 and z^6 , respectively. This suffices since the anomalies cancel for each E_8 gauge group, and also we are interested in the local structure of the singularity. x and y are then taken to be sections of $\mathcal{O}(2(-K_{\mathbb{F}_n} - C_0))$ and $\mathcal{O}(3(-K_{\mathbb{F}_n} - C_0))$, where C_0 is a divisor class with $C_0^2 = -n$, satisfying $-K_{\mathbb{F}_n} = 2C_0 + (2+n)f$ with the fiber class f . Similar modifications are necessary for $f(z, z')$ and $g(z, z')$. This deviation from the anti-canonical class (and hence from a Calabi-Yau) is because we consider a rational-elliptic-surface fibration.

The Weierstrass equation (2.1) with (2.2) can be written in Tate's form as

$$y'^2 + x'^3 + \alpha_4 z^4 x' + \alpha_6 z^6 + a_0 z^5 + a_2 z^3 x' + a_3 z^2 y' + a_4 z x'^2 + a_5 x' y' = 0 \quad (2.3)$$

with

$$\begin{aligned} a_5 &= 2\sqrt{3}i h_{n+2}, \\ a_4 &= -6H_{n+4}, \\ a_3 &= 4\sqrt{3}i q_{n+6}, \\ a_2 &= f_{n+8}, \\ a_0 &= g_{n+12} - 2H_{n+4} f_8, \\ \alpha_4 &= f_8, \\ \alpha_6 &= g_{12}. \end{aligned} \quad (2.4)$$

For completeness we write x, y in (2.1) in terms of x', y' in (2.3):

$$\begin{aligned} x &= x' + \frac{1}{3} \left(a_4 z - \frac{1}{4} a_5^2 \right), \\ y &= i \left(y' + \frac{1}{2} (a_5 x' + a_3 z^2) \right). \end{aligned} \quad (2.5)$$

$SU(6)$

To obtain an equation for $SU(6)$ gauge group, which yields half-hypermultiplets, we set [7]

$$\begin{aligned}
h_{n+2} &= t_r h_{n+2-r}, \\
H_{n+4} &= t_r H_{n+4-r}, \\
q_{n+6} &= u_{r+4} h_{n+2-r}, \\
f_{n+8} &= t_r f_{n+8-r} - 12u_{r+4} H_{n+4-r}, \\
g_{n+12} &= 2(u_{r+4} f_{n-r+8} + f_8 t_r H_{n-r+4}).
\end{aligned} \tag{2.6}$$

Then the spectral cover factorizes as

$$\begin{aligned}
0 &= a_0 z^5 + a_2 z^3 x' + a_3 z^2 y' + a_4 z x'^2 + a_5 x' y' \\
&= (x' t_r + 2z^2 u_{r+4}) \left(z^3 f_{n-r+8} + 2i\sqrt{3} y' h_{n-r+2} - 6z x' H_{n-r+4} \right),
\end{aligned} \tag{2.7}$$

indicating that the $SU(5)$ instanton is reduced to an $SU(3) \times SU(2)$ instanton in the heterotic dual, at the same time the Mordell-Weil rank of the rational elliptic surface is reduced. The Mordell-Weil lattice is No.15 in the Oguiso-Shioda classification [25]. In this specification $f(z, z')$ and $g(z, z')$ become

$$\begin{aligned}
f_{SU(6)}(z, z') &= -3t_r^4 h_{n-r+2}^4 + 12zt_r^3 h_{n-r+2}^2 H_{n-r+4} + z^2 (12t_r u_{r+4} h_{n-r+2}^2 - 12t_r^2 H_{n-r+4}^2) \\
&\quad + z^3 (t_r f_{n-r+8} - 12u_{r+4} H_{n-r+4}) + f_8 z^4,
\end{aligned} \tag{2.8}$$

$$\begin{aligned}
g_{SU(6)}(z, z') &= 2t_r^6 h_{n-r+2}^6 - 12zt_r^5 h_{n-r+2}^4 H_{n-r+4} \\
&\quad + z^2 (24t_r^4 h_{n-r+2}^2 H_{n-r+4}^2 - 12t_r^3 u_{r+4} h_{n-r+2}^4) \\
&\quad + z^3 (-t_r^3 f_{n-r+8} h_{n-r+2}^2 + 36t_r^2 u_{r+4} h_{n-r+2}^2 H_{n-r+4} - 16t_r^3 H_{n-r+4}^3) \\
&\quad + z^4 (-f_8 t_r^2 h_{n-r+2}^2 + 2t_r^2 f_{n-r+8} H_{n-r+4} + 12u_{r+4}^2 h_{n-r+2}^2 - 24t_r u_{r+4} H_{n-r+4}^2) \\
&\quad + z^5 (2f_8 t_r H_{n-r+4} + 2u_{r+4} f_{n-r+8}) + g_{12} z^6.
\end{aligned} \tag{2.9}$$

The discriminant reads

$$\begin{aligned}
\Delta_{SU(6)} &= 9z^6 t_r^3 h_{n-r+2}^4 \left[t_r^3 (12g_{12} h_{n-r+2}^2 - f_{n-r+8}^2) \right. \\
&\quad \left. + t_r^2 (-24f_8 u_{r+4} h_{n-r+2}^2 - 24u_{r+4} f_{n-r+8} H_{n-r+4}) \right. \\
&\quad \left. - 144t_r u_{r+4}^2 H_{n-r+4}^2 - 96u_{r+4}^3 h_{n-r+2}^2 \right] + O(z^7).
\end{aligned} \tag{2.10}$$

Thus the Weierstrass model with (2.8),(2.9) indeed has a codimension-one $SU(6)$ singularity along $z = 0$.

The zero loci of t_r are the points where the $SU(6)$ singularity is enhanced to E_6 , those of h_{n-r+2} are the ones to D_6 , and those of the remaining factor of degree $2n+r+16$ are the ones to A_6 . They respectively yield r half-hypermultiplets in **20**, $n-r+2$ hypermultiplets in **15** and $2n+r+16$ hypermultiplets in **6**.

The number of the complex structure moduli is $3n - r + 21$, which satisfies the anomaly-free constraint for one of the E_8 factors [7]

$$\begin{aligned} n_H - n_V &= 20 \cdot \frac{r}{2} + 15(n - r + 2) + 6(2n + r + 16) + 3n - r + 21 - 35 \\ &= 30n + 112. \end{aligned} \quad (2.11)$$

Note that this condition does not hold if the multiplets in **20** are ordinary hypermultiplets.

SO(12)

To further obtain an equation for $SO(12)$ gauge group, one only needs to set $h_{n+2-r} = 0$ in (2.6). The spectral cover is now

$$(x't_r + 2z^2u_{r+4}) \left(x'H_{n-r+4} - \frac{1}{6}z^2f_{n-r+8} \right) = 0. \quad (2.12)$$

These factors are in the same form, corresponding to two $SU(2)$'s of the instanton gauge group of the heterotic theory. The Mordell-Weil lattice is No.26 in [25].

Then $f(z, z')$ and $g(z, z')$ are

$$f_{SO(12)}(z, z') = -12z^2t_r^2H_{n-r+4}^2 + z^3(t_rf_{n-r+8} - 12u_{r+4}H_{n-r+4}) + f_8z^4, \quad (2.13)$$

$$\begin{aligned} g_{SO(12)}(z, z') &= -16z^3t_r^3H_{n-r+4}^3 + 2z^4(t_r^2f_{n-r+8}H_{n-r+4} - 12t_ru_{r+4}H_{n-r+4}^2) \\ &\quad + 2z^5(f_8t_rH_{n-r+4} + u_{r+4}f_{n-r+8}) + g_{12}z^6. \end{aligned} \quad (2.14)$$

The discriminant is

$$\Delta_{SO(12)} = -36z^8t_r^2H_{n-r+4}^2(t_rf_{n-r+8} + 12u_{r+4}H_{n-r+4})^2 + O(z^9). \quad (2.15)$$

The zero loci of both t_r and H_{n-r+4} give rise to E_7 singularities to yield $n + 4$ half-hypermultiplets. The loci of the remaining factor are A_7 singularities, giving $n + 8$ hypers in **12**. With additional neutral hypermultiplets from the $2n + 18$ complex structure moduli, we have

$$\begin{aligned} n_H - n_V &= 32 \cdot \frac{n+4}{2} + 12(n+8) + 2n+18 - 66 \\ &= 30n + 112 \end{aligned} \quad (2.16)$$

as it should be. Again, if **32** is not a half-hyper, the anomaly does not cancel.

E₇

Finally, the E_7 model can be obtained by setting $h_{n+2} = H_{n+4} = q_{n+6} = 0$ in the $SU(5)$ model. The gauge group of the heterotic vector bundle is $SU(2)$. The Mordell-Weil lattice is No.43 in [25]. $f(z, z')$ and $g(z, z')$ are simply given by

$$f_{E_7}(z, z') = f_{n+8}z^3 + f_8z^4, \quad (2.17)$$

$$g_{E_7}(z, z') = g_{n+12}z^5 + g_{12}z^6. \quad (2.18)$$

The discriminant

$$\Delta_{E_7} = 4f_{n+8}^3 z^9 + O(z^{10}) \quad (2.19)$$

implies that $n + 8$ half-hypermultiplets in **56** of E_7 arise. Again they must be half-hyper as

$$\begin{aligned} n_H - n_V &= 56 \cdot \frac{n+8}{2} + 2n + 21 - 133 \\ &= 30n + 112. \end{aligned} \quad (2.20)$$

3 $SO(12) \rightarrow E_7$

We consider a Weierstrass model on a base two-fold B_2 with local coordinates $\{z, s\}$, where the codimension-one singularity arises along $z = 0$ and the codimension-two singularity arises at $s = 0$ on the $z = 0$ complex line. s corresponds to z' in the previous section.

3.1 Incomplete resolution: Blowing up p_1 first

3.1.1 Blowing up process

We consider a concrete Weierstrass model of incomplete resolution by setting ⁴ $H_{n-r+4} = s$, $t_r = -\frac{1}{2}$, $f_{n-r+8} = -2$ and $u_{r+4} = f_8 = g_{12} = 0$ in (2.13) and (2.14):

$$\Phi(x, y, z, s) = -y^2 + x^3 + f(z, s)x + g(z, s) = 0, \quad (3.1)$$

where

$$\begin{aligned} f(z, s) &= -3s^2 z^2 + z^3, \\ g(z, s) &= 2s^3 z^3 - sz^4. \end{aligned} \quad (3.2)$$

At $s \neq 0$, the orders of f , g and the discriminant Δ in z are $(2, 3, 8)$, while at $s = 0$, they satisfy $(3, \geq 5, 9)$. Therefore (3.2) describes the enhancement $I_2^* \rightarrow III^*$ ($SO(12) \rightarrow E_7$) of the Kodaira type, satisfying the requirement.

1st blow up With (3.2), the equation (3.1) reads

$$\Phi(x, y, z, s) = xz^2(z - 3s^2) + sz^3(2s^2 - z) + x^3 - y^2 = 0. \quad (3.3)$$

(3.3) has a codimension-one singularity at $p_0 \equiv (0, 0, 0, s)$. We blow up this by replacing the complex line $(x, y, z) = (0, 0, 0)$ with $\mathbb{P}^2 \times \mathbb{C}$ in \mathbb{C}^4 by passing to the following charts corresponding to three affine patches of \mathbb{P}^2 for fixed s :

Chart 1_x

$$\begin{aligned} \Phi(x, xy_1, xz_1, s) &= x^2 \Phi_x(x, y_1, z_1, s), \\ \Phi_x(x, y_1, z_1, s) &= x^2 (z_1^3 - sz_1^4) + x (sz_1 - 1)^2 (2sz_1 + 1) - y_1^2. \\ \mathcal{C}_{p_0} \text{ in } 1_x &: x = 0, \quad y_1 = 0. \\ \text{Singularities} &: (x, y_1, z_1, s) = (0, 0, \frac{1}{s}, s), (0, 0, -\frac{1}{2s}, s). \end{aligned} \quad (3.4)$$

⁴The same model is obtained by setting $t_r = s$, $H_{n-r+4} = -\frac{1}{2}$, $u_{r+4} = \frac{1}{6}$ and $f_{n-r+8} = f_8 = g_{12} = 0$.

These singularities are of codimension one, which we refer to as p_1 and q_1 , respectively. \mathcal{C}_{p_0} is the exceptional curve at fixed s .

Chart 1_y

$$\begin{aligned}\Phi(x_1y, y, yz_1, s) &= y^2\Phi_y(x_1, y, z_1, s), \\ \Phi_y(x_1, y, z_1, s) &= 2s^3yz_1^3 + x_1yz_1^2(yz_1 - 3s^2) - sy^2z_1^4 + x_1^3y - 1. \\ \mathcal{C}_{p_0} \text{ in } 1_y &: \text{Invisible in this patch.} \\ \text{Singularities} &: \text{None.}\end{aligned}\tag{3.5}$$

In chart 1_y , the exceptional curve cannot be seen and there is no singularity.

Chart 1_z

$$\begin{aligned}\Phi(x_1z, y_1z, z, s) &= z^2\Phi_z(x_1, y_1, z, s), \\ \Phi_z(x_1, y_1, z, s) &= z(2s^3 - 3s^2x_1 - sz + x_1^3 + x_1z) - y_1^2. \\ \mathcal{C}_{p_0} \text{ in } 1_z &: z = 0, \quad y_1 = 0. \\ \text{Singularities} &: (x_1, y_1, z, s) = (s, 0, 0, s), (-2s, 0, 0, s).\end{aligned}\tag{3.6}$$

The first singularity is p_1 , while the second is q_1 .

2nd blow up By the 1st blow up we found two singularities. There are two ways to resolve them; either we blow up p_1 first, or q_1 first. In this section we blow up p_1 first.

In order to blow up the singularity p_1 in $\Phi_z(x_1, y_1, z, s) = 0$, we shift the coordinate x_1 so that the position of the singularity becomes $(0, 0, 0, s)$:

$$\Psi_z(\tilde{x}_1, y_1, z, s) \equiv \Phi_z(\tilde{x}_1 + s, y_1, z, s).\tag{3.7}$$

The singularities of $\Psi_z(\tilde{x}_1, y_1, z, s) = 0$ are now at $(0, 0, 0, s)$ ($= p_1$) and $(-3s, 0, 0, s)$ ($= q_1$). We blow up the singularity of $\Psi_z(\tilde{x}_1, y_1, z, s) = 0$ at $(0, 0, 0, s)$.

Chart 2_{zx}

$$\begin{aligned}\Psi_z(\tilde{x}_1, \tilde{x}_1y_2, \tilde{x}_1z_2, s) &= \tilde{x}_1^2\Psi_{zx}(\tilde{x}_1, y_2, z_2, s), \\ \Psi_{zx}(\tilde{x}_1, y_2, z_2, s) &= \tilde{x}_1z_2(3s + \tilde{x}_1 + z_2) - y_2^2. \\ \mathcal{C}_{p_1} \text{ in } 2_{zx} &: \tilde{x}_1 = 0, \quad y_2 = 0. \\ \text{Singularities} &: (\tilde{x}_1, y_2, z_2, s) = (0, 0, 0, s)(= p_2), (0, 0, -3s, s)(= r_2), \\ &\quad (-3s, 0, 0, s)(= q_1).\end{aligned}\tag{3.8}$$

We find three singularities in this chart and name them as shown in the parentheses.

Chart 2_{zy} In this chart, we find no singularity so we omit the details of Ψ_{zy} .

Chart 2_{zz}

$$\begin{aligned}\Psi_z(x_2z, y_2z, z, s) &= z^2\Psi_{zz}(x_2, y_2, z, s), \\ \Psi_{zz}(x_2, y_2, z, s) &= x_2z(3sx_2 + x_2^2z + 1) - y_2^2. \\ \mathcal{C}_{p_1} \text{ in } 2_{zz} &: z = 0, \quad y_2 = 0. \\ \text{Singularities} &: (x_2, y_2, z, s) = (0, 0, 0, s)(= q_2), \left(-\frac{1}{3s}, 0, 0, s\right)(= r_2).\end{aligned}\tag{3.9}$$

We observe two singularities. The former (q_2) is one which can only be seen in this chart, while the latter (r_2) is already seen in chart 2_{zx} .

Here the process branches off in three ways depending on which of the three singularities p_2 , r_2 and q_1 in chart 2_{zx} is blown up next. Although they are separated for $s \neq 0$, they coincide with each other at $s = 0$ (see (3.8)). For this reason, changing the order of blowing up these three singularities changes the subsequent geometries. In this section, we consider the case p_2 is blown up next. On the other hand, q_2 in chart 2_{zz} is separated with the other three singularities even at $s = 0$, and hence it can be independently blown up. We leave the blow-up of q_2 until later and proceed with blowing up p_2 .

3rd blow up at p_2 We blow up p_2 in chart 2_{zx} :

Chart 3_{zxx}

$$\begin{aligned}\Psi_{zx}(\tilde{x}_1, \tilde{x}_1 y_3, \tilde{x}_1 z_3, s) &= \tilde{x}_1^2 \Psi_{zxx}(\tilde{x}_1, y_3, z_3, s), \\ \Psi_{zxx}(\tilde{x}_1, y_3, z_3, s) &= z_3(3s + \tilde{x}_1 z_3 + \tilde{x}_1) - y_3^2. \\ \mathcal{C}_{p_2} \text{ in } 3_{zxx} &: \tilde{x}_1 = 0, \quad y_3^2 = 3s z_3. \\ \text{Singularities} &: (\tilde{x}_1, y_3, z_3, s) = (-3s, 0, 0, s) (= q_1).\end{aligned}\tag{3.10}$$

Chart 3_{zxy} Regular.

Chart 3_{zzz}

$$\begin{aligned}\Psi_{zx}(x_3 z_2, y_3 z_2, z_2, s) &= z_2^2 \Psi_{zzz}(x_3, y_3, z_2, s), \\ \Psi_{zzz}(x_3, y_3, z_2, s) &= 3s x_3 + x_3(x_3 + 1)z_2 - y_3^2. \\ \mathcal{C}_{p_2} \text{ in } 3_{zzz} &: z_2 = 0, \quad y_3^2 = 3s x_3. \\ \text{Singularities} &: (x_3, y_3, z_2, s) = (0, 0, -3s, s) (= r_2).\end{aligned}\tag{3.11}$$

The remaining singularities are resolved by blowing up q_1 , r_2 and q_2 , which are all codimension one. q_1 and r_2 , which were overlapping at $s = 0$ in chart 2_{zx} before blowing up p_2 , are now contained in different charts 3_{zxx} and 3_{zzz} , respectively, and are separated even at $s = 0$. Also, q_2 stays in chart 2_{zz} and never coincides with them. Therefore, the remaining three singularities are all separated with each other for any s and can be independently blown up. The procedure is similar as before and is easily done, but for later use, we complete the process here and present the relevant results. After blowing up q_1 in chart 3_{zxx} and r_2 in chart 3_{zzz} , we return to chart 2_{zz} and blow up q_2 . These blow-ups do not cause any new singularities.

4th blow up at q_1 To blow up q_1 in chart 3_{zxx} , we shift the \tilde{x}_1 coordinate so that q_1 is at the origin:

$$\Sigma_{zxx}(\tilde{\tilde{x}}_1, y_3, z_3, s) \equiv \Psi_{zxx}(\tilde{\tilde{x}}_1 - 3s, y_3, z_3, s).\tag{3.12}$$

Chart 4_{zxxx}

$$\begin{aligned}\Sigma_{zxx}(\tilde{\tilde{x}}_1, \tilde{\tilde{x}}_1 y_4, \tilde{\tilde{x}}_1 z_4, s) &= \tilde{\tilde{x}}_1^2 \Sigma_{zxxx}(\tilde{\tilde{x}}_1, y_4, z_4, s), \\ \Sigma_{zxxx}(\tilde{\tilde{x}}_1, y_4, z_4, s) &= -y_4^2 + z_4(1 + \tilde{\tilde{x}}_1 z_4 - 3z_4 s). \\ \mathcal{C}_{q_1} \text{ in } 4_{zxxx} &: \tilde{\tilde{x}}_1 = 0, \quad y_4^2 = z_4(1 - 3z_4 s).\end{aligned}\tag{3.13}$$

Chart 4_{zxy} We omit the details.

Chart 4_{zxxz}

$$\begin{aligned}\Sigma_{zxx}(x_4z_3, y_4z_3, z_3, s) &= z_3^2 \Sigma_{zxxz}(x_4, y_4, z_3, s), \\ \Sigma_{zxxz}(x_4, y_4, z_3, s) &= -y_4^2 + x_4(1 + z_3) - 3s, \\ \mathcal{C}_{q_1} \text{ in } 4_{zxxz} &: z_3 = 0, \quad y_4^2 = x_4 - 3s.\end{aligned}\tag{3.14}$$

4th blow up at r_2 To blow up r_2 in chart 3_{zxxz} , we shift the z_2 coordinate so that r_2 is at the origin:

$$\Sigma_{zxxz}(x_3, y_3, \tilde{z}_2, s) \equiv \Psi_{zxxz}(x_3, y_3, \tilde{z}_2 - 3s, s).\tag{3.15}$$

Chart 4_{zxxz}

$$\begin{aligned}\Sigma_{zxxz}(x_3, x_3y_4, x_3z_4, s) &= x_3^2 \Sigma_{zxxz}(x_3, y_4, z_4, s), \\ \Sigma_{zxxz}(x_3, y_4, z_4, s) &= -y_4^2 + z_4(1 + x_3) - 3s, \\ \mathcal{C}_{r_2} \text{ in } 4_{zxxz} &: x_3 = 0, \quad y_4^2 = z_4 - 3s.\end{aligned}\tag{3.16}$$

Chart 4_{zzy} We omit the details.

Chart 4_{zxxz}

$$\begin{aligned}\Sigma_{zxxz}(x_4\tilde{z}_2, y_4\tilde{z}_2, \tilde{z}_2, s) &= \tilde{z}_2^2 \Sigma_{zxxz}(x_4, y_4, \tilde{z}_2, s), \\ \Sigma_{zxxz}(x_4, y_4, \tilde{z}_2, s) &= -y_4^2 + x_4 + x_4^2(\tilde{z}_2 - 3s), \\ \mathcal{C}_{r_2} \text{ in } 4_{zxxz} &: \tilde{z}_2 = 0, \quad y_4^2 = x_4 - 3x_4^2s.\end{aligned}\tag{3.17}$$

3rd blow up at q_2 Finally, we go back to chart 2_{zz} and blow up q_2 (3.9):

Chart 3_{zxx}

$$\begin{aligned}\Psi_{zz}(x_2, x_2y_3, x_2z_3, s) &= x_2^2 \Psi_{zxx}(x_2, y_3, z_3, s), \\ \Psi_{zxx}(x_2, y_3, z_3, s) &= -y_3^2 + z_3(1 + x_2^3z_3 + 3x_2s), \\ \mathcal{C}_{q_2} \text{ in } 3_{zxx} &: x_2 = 0, \quad y_3^2 = z_3.\end{aligned}\tag{3.18}$$

Chart 3_{zzy} We omit the details.

Chart 3_{zzz}

$$\begin{aligned}\Psi_{zz}(x_3z, y_3z, z, s) &= z^2 \Psi_{zzz}(x_3, y_3, z, s), \\ \Psi_{zzz}(x_3, y_3, z, s) &= -y_3^2 + x_3 + x_3^3z^3 + 3x_3^2zs, \\ \mathcal{C}_{q_2} \text{ in } 3_{zzz} &: z = 0, \quad y_3^2 = x_3.\end{aligned}\tag{3.19}$$

The whole process of blowing up is summarized in Table 1.

Table 1. $SO(12) \rightarrow E_7$: Incomplete case when p_1 is blown up first and then p_2 is blown up ($p_0 \rightarrow p_1 \rightarrow p_2$). The singularities appearing at each step of the process are shown with their homogeneous coordinates on \mathbb{P}^2 . The ones marked by a circle are those blown up at the subsequent processes. p_0 denotes the original singularity on the fiber. The notes in the parentheses (such as $\tilde{x}_1 = -3s$ for q_1) imply that they are not generically (*i.e.* unless $s \neq 0$) the points on the \mathbb{P}^2 arising at the respective step of the blowing-up process.

	1st blow up	2nd blow up	3rd blow up	4th blow up
$\textcircled{p_0} \rightarrow$	$\textcircled{p_1}(s : 0 : 1) \rightarrow$ $q_1(-2s : 0 : 1)$	$\textcircled{p_2}(1 : 0 : 0)$ (in 2_{zx}) \rightarrow $q_1(1 : 0 : 0)(\tilde{x}_1 = -3s)$ $r_2(1 : 0 : -3s)$ $\textcircled{q_2}(0 : 0 : 1)$ (in 2_{zz}) \rightarrow	regular $\textcircled{q_1}(1 : 0 : 0)(\tilde{x}_1 = -3s) \rightarrow$ $\textcircled{r_2}(0 : 0 : 1)(z_2 = -3s) \rightarrow$ regular	regular regular

3.1.2 Intersection patterns at $s \neq 0$ and $s = 0$

Through the blowing up process, we have obtained six exceptional curves \mathcal{C}_I ($I \in \{p_0, p_1, p_2, q_1, r_2, q_2\}$) at general s . For given \mathcal{C} , we define the corresponding exceptional curve δ as the $s \rightarrow 0$ limit of \mathcal{C} in the chart where \mathcal{C} originally is defined. One can then show that the intersection pattern of $\{\mathcal{C}_I\}$ at $s \neq 0$ and that of $\{\delta_I\}$ at $s = 0$ are D_6 and A_6 , respectively.

Let us present the detail of the derivation. Suppose \mathcal{C} and δ arise from some blow-up and are defined in chart A , while \mathcal{C}' and δ' arise from a subsequent blow-up and are defined in chart A' . In order to see how \mathcal{C} and δ intersect with \mathcal{C}' and δ' , one has to locate their positions in the same chart. This is done by lifting up \mathcal{C} and δ from chart A to chart A' .

Let us start from defining δ_{p_0} by \mathcal{C}_{p_0} in chart 1 (take chart 1_z : see (3.6)) as

$$\text{Chart } 1_z \quad \mathcal{C}_{p_0} : z = 0, y_1 = 0 \quad , \quad \delta_{p_0} : z = 0, y_1 = 0. \quad (3.20)$$

Since \mathcal{C}_{p_0} does not depend on s , δ_{p_0} has the same form as \mathcal{C}_{p_0} .

Next, we lift them up in chart 2_{zx} . Lifting up is done by transforming the coordinates from chart A to chart A' : in this case, from chart 1_z to chart 2_{zx} . The relation between these charts is $(\tilde{x}_1, y_1, z) = (\tilde{x}_1, \tilde{x}_1 y_2, \tilde{x}_1 z_2)$ (see (3.7) and (3.8)). Substituting it into (3.20), we see that \mathcal{C}_{p_0} and δ_{p_0} are written as $\tilde{x}_1 z_2 = 0$, $\tilde{x}_1 y_2 = 0$. It is reduced to $z_2 = 0$, $y_2 = 0$, because $\tilde{x}_1 (= x_1 - s)$ parameterizes \mathcal{C}_{p_0} and δ_{p_0} , and thus takes a non-zero value. Together with \mathcal{C}_{p_1} and δ_{p_1} defined in chart 2_{zx} (see (3.8)), we have

$$\begin{aligned} \text{Chart } 2_{zx} \quad \mathcal{C}_{p_1} : \tilde{x}_1 = 0, y_2 = 0 \quad , \quad \delta_{p_1} : \tilde{x}_1 = 0, y_2 = 0, \\ \mathcal{C}_{p_0} : z_2 = 0, y_2 = 0 \quad , \quad \delta_{p_0} : z_2 = 0, y_2 = 0. \end{aligned} \quad (3.21)$$

Thus \mathcal{C}_{p_0} (δ_{p_0}) intersects with \mathcal{C}_{p_1} (δ_{p_1}) in this chart:

$$\mathcal{C}_{p_0} \cdot \mathcal{C}_{p_1} \neq 0 \quad , \quad \delta_{p_0} \cdot \delta_{p_1} \neq 0. \quad (3.22)$$

Comparing the locus of the singularities (3.8) with the positions of \mathcal{C}_i (3.21), we find that $p_2 = (0, 0, 0, s)$ is located at the intersection point of \mathcal{C}_{p_0} and \mathcal{C}_{p_1} , while $q_1 = (-3s, 0, 0, s)$

and $r_2 = (0, 0, -3s, s)$ are on \mathcal{C}_{p_0} and \mathcal{C}_{p_1} , respectively. As $s \rightarrow 0$, q_1 and r_2 approach p_2 . At $s = 0$, they overlap with p_2 at the intersection point of δ_{p_0} and δ_{p_1} . Similarly, in chart 2_{zz} , we have

$$\begin{aligned} \text{Chart } 2_{zz} \quad \mathcal{C}_{p_1} : z = 0, y_2 = 0 \quad , \quad \delta_{p_1} : z = 0, y_2 = 0, \\ \mathcal{C}_{p_0} : \text{Invisible} \quad \quad \quad , \quad \delta_{p_0} : \text{Invisible}. \end{aligned} \quad (3.23)$$

The reason why \mathcal{C}_{p_0} and δ_{p_0} are invisible in chart 2_{zz} is as follows. As seen from (3.7) and (3.9), the coordinates of 1_z and 2_{zz} are related by $(\tilde{x}_1, y_1, z) = (x_2z, y_2z, z)$. Then \mathcal{C}_{p_0} and δ_{p_0} (3.20) are given by $(x_2z, y_2z, z) = (\tilde{x}_1 \neq 0, 0, 0)$. It yields $x_2 = \infty$, which means that the lift-ups of \mathcal{C}_{p_0} and δ_{p_0} cannot be seen in the finite region of chart 2_{zz} . The locus of the singularities q_2 and r_2 can be read from (3.9) and (3.23). For $s \neq 0$, both of them are on \mathcal{C}_{p_1} . At $s = 0$, q_2 stays on δ_{p_1} , whereas r_2 has gone to infinity. The positions of the exceptional curves and the singularities in chart 2 are schematically depicted in the leftmost column of Figure 1.

In the same way, lifting up from chart 2_{zx} to chart 3_{zxx} yields

$$\begin{aligned} \text{Chart } 3_{zxx} \quad \mathcal{C}_{p_2} : \tilde{x}_1 = 0, y_3^2 = 3sz_3 \quad , \quad \delta_{p_2} : \tilde{x}_1 = 0, y_3 = 0, \\ \mathcal{C}_{p_1} : \text{Invisible} \quad \quad \quad , \quad \delta_{p_1} : \text{Invisible}, \\ \mathcal{C}_{p_0} : z_3 = 0, y_3 = 0 \quad \quad \quad , \quad \delta_{p_0} : z_3 = 0, y_3 = 0. \end{aligned} \quad (3.24)$$

This leads to

$$\mathcal{C}_{p_0} \cdot \mathcal{C}_{p_2} \neq 0 \quad , \quad \delta_{p_0} \cdot \delta_{p_2} \neq 0. \quad (3.25)$$

The singularity $q_1 = (-3s, 0, 0, s)$ (3.10) is contained in \mathcal{C}_{p_0} but not in \mathcal{C}_{p_2} for $s \neq 0$, whereas it is located at the intersection point of δ_{p_0} and δ_{p_2} at $s = 0$. Lift-up from chart 2_{zx} to chart 3_{zxz} yields

$$\begin{aligned} \text{Chart } 3_{zxz} \quad \mathcal{C}_{p_2} : z_2 = 0, y_3^2 = 3s\tilde{x}_3 \quad , \quad \delta_{p_2} : z_2 = 0, y_3 = 0, \\ \mathcal{C}_{p_1} : \tilde{x}_3 = 0, y_3 = 0 \quad \quad \quad , \quad \delta_{p_1} : \tilde{x}_3 = 0, y_3 = 0, \\ \mathcal{C}_{p_0} : \text{Invisible} \quad \quad \quad , \quad \delta_{p_0} : \text{Invisible}, \end{aligned} \quad (3.26)$$

and hence

$$\mathcal{C}_{p_1} \cdot \mathcal{C}_{p_2} \neq 0 \quad , \quad \delta_{p_1} \cdot \delta_{p_2} \neq 0. \quad (3.27)$$

The singularity $r_2 = (0, 0, -3s, s)$ (3.11) is contained in \mathcal{C}_{p_1} but not in \mathcal{C}_{p_2} for $s \neq 0$, whereas it is located at the intersection point of δ_{p_1} and δ_{p_2} at $s = 0$. The positions of these objects in chart 3 (together with the objects in chart 2_{zz}) are depicted in the second column of Figure 1.

As seen in the previous subsection, the remaining three singularities q_1 in chart 3_{zxx} , r_2 in chart 3_{zxz} and q_2 in chart 2_{zz} are independently blown up. Here we consider the blow-up of q_1 and lift all the information of chart 3_{zxx} (3.24) up in chart 4. In chart 4_{zxxx} (3.13),

the result is

$$\begin{array}{ll}
\text{Chart } 4_{zxxx} & \mathcal{C}_{q_1} : \tilde{x}_1 = 0, y_4^2 = z_4 - 3z_4^2s \quad , \quad \delta_{q_1} : \tilde{x}_1 = 0, y_4^2 = z_4, \\
& \mathcal{C}_{p_2} : \tilde{x}_1 - 3s = 0, y_4^2 = z_4 \quad , \quad \delta_{p_2} : \text{Invisible}, \\
& \mathcal{C}_{p_1} : \text{Invisible} \quad , \quad \delta_{p_1} : \text{Invisible}, \\
& \mathcal{C}_{p_0} : z_4 = 0, y_4 = 0 \quad , \quad \delta_{p_0} : z_4 = 0, y_4 = 0. \quad (3.28)
\end{array}$$

We will briefly explain how the forms of \mathcal{C}_{p_2} and δ_{p_2} are obtained. The coordinates of chart 3_{zxx} and 4_{zxxx} are related by (see (3.12) and (3.13))

$$(\tilde{x}_1 + 3s, y_3, z_3) = (\tilde{x}_1, \tilde{x}_1 y_4, \tilde{x}_1 z_4). \quad (3.29)$$

Substituting it into (3.24), we have

$$\mathcal{C}_{p_2} : \tilde{x}_1 - 3s = 0, \tilde{x}_1^2 y_4^2 = 3s \tilde{x}_1 z_4. \quad (3.30)$$

The second equation is rewritten by using the first equation as $\tilde{x}_1^2 y_4^2 = \tilde{x}_1^2 z_4$. Since $s \neq 0$, the first equation leads $\tilde{x}_1 \neq 0$. Thus the second equation is reduced to $y_4^2 = z_4$. To see the form of δ_{p_2} , we set $s = 0$ in (3.29). Then, from (3.24), δ_{p_2} is given by $(\tilde{x}_1, \tilde{x}_1 y_4, \tilde{x}_1 z_4) = (0, 0, z_3 \neq 0)$. It yields $z_4 = \infty$ and is invisible in chart 4_{zxxx} . From (3.28), one can see the following intersections in this chart:

$$\mathcal{C}_{p_0} \cdot \mathcal{C}_{p_2} \neq 0, \mathcal{C}_{p_0} \cdot \mathcal{C}_{q_1} \neq 0 \quad , \quad \delta_{p_0} \cdot \delta_{q_1} \neq 0. \quad (3.31)$$

In chart 4_{zxyy} , one can show that \mathcal{C}_{p_0} is invisible as well, and no intersection can be seen. In chart 4_{zxxz} (3.14), we have

$$\begin{array}{ll}
\text{Chart } 4_{zxxz} & \mathcal{C}_{q_1} : z_3 = 0, y_4^2 = x_4 - 3s \quad , \quad \delta_{q_1} : z_3 = 0, y_4^2 = x_4, \\
& \mathcal{C}_{p_2} : x_4 z_3 - 3s = 0, y_4^2 = x_4 \quad , \quad \delta_{p_2} : x_4 = 0, y_4 = 0, \\
& \mathcal{C}_{p_1} : \text{Invisible} \quad , \quad \delta_{p_1} : \text{Invisible}, \\
& \mathcal{C}_{p_0} : \text{Invisible} \quad , \quad \delta_{p_0} : \text{Invisible}, \quad (3.32)
\end{array}$$

where $(\tilde{x}_1 + 3s, y_3, z_3) = (x_4 z_3, y_4 z_3, z_3)$. \mathcal{C}_{q_1} does not intersect with \mathcal{C}_{p_2} , whereas δ_{q_1} intersects with δ_{p_2} :

$$\delta_{p_2} \cdot \delta_{q_1} \neq 0. \quad (3.33)$$

There is no singularity in these charts. The positions of the exceptional curves and the singularities after this blow-up are given in the third column in Figure 1. Since q_1 was on \mathcal{C}_{p_0} but not on \mathcal{C}_{p_2} in chart 3, \mathcal{C}_{q_1} intersects only with \mathcal{C}_{p_0} in chart 4. On the other hand, q_1 was on the intersection of δ_{p_0} and δ_{p_2} , and hence δ_{q_1} bridges them after the blow-up.

The intersections after blowing up the remaining two singularities r_2 and q_2 are obtained in a similar manner. The result is given in the rightmost column in Figure 1. The final intersection patterns for $s \neq 0$ and $s = 0$ are the D_6 and A_6 Dynkin diagrams, respectively (see also Figure 2 in the next subsection; the meaning of the triangular node in A_6 will be clarified there).

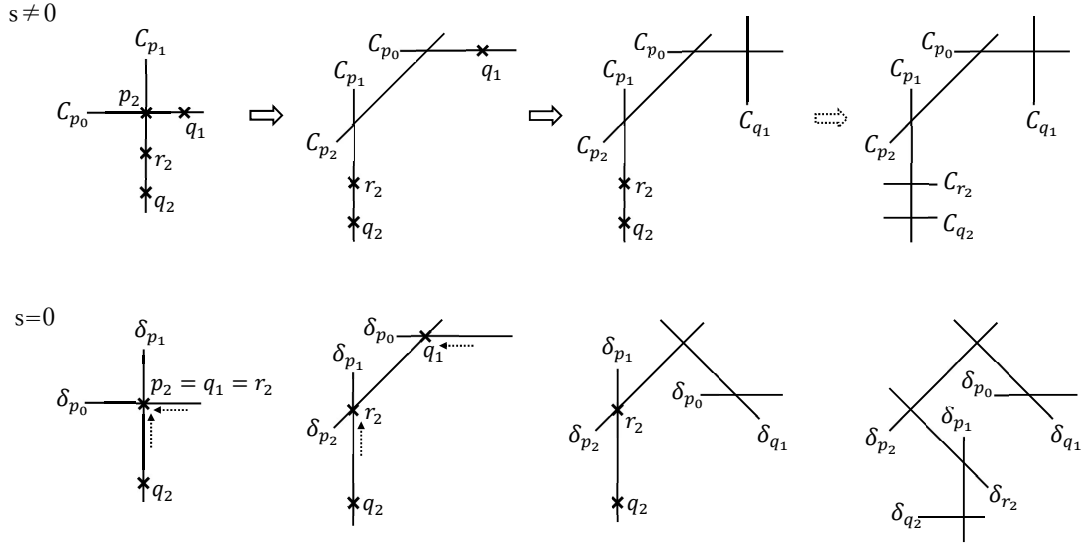


Figure 1. Exceptional curves and singularities of $SO(12) \rightarrow E_7 : p_0 \rightarrow p_1 \rightarrow p_2$ case.

3.1.3 Intersection diagram at $s = 0$: Transmutation of a root into a weight

In this subsection, we examine how D_6 Dynkin diagram at $s \neq 0$ becomes A_6 at $s = 0$; in other words, how the sets $\{\mathcal{C}_I\}$ and $\{\delta_I\}$ are related. For this, as discovered in [11], it is important to know the $s \rightarrow 0$ limit of \mathcal{C} , which we write $\lim_{s \rightarrow 0} \mathcal{C}$. Here, we give a detailed explanation how this limit is explicitly calculated. It is worth noting that $\lim_{s \rightarrow 0} \mathcal{C}$ does not necessarily coincide with δ . Suppose \mathcal{C} and δ are defined in chart A , while \mathcal{C}' and δ' are defined in a “deeper” chart A' . By definition, $\lim_{s \rightarrow 0} \mathcal{C} = \delta$ in chart A . However, after \mathcal{C} and δ are lifted up in chart A' , \mathcal{C} coexists with δ' and hence $\lim_{s \rightarrow 0} \mathcal{C}$ may contain δ' . This can happen only after the lift-up. That is, lifting up and taking $s \rightarrow 0$ limit do not commute in general, and we should take $s \rightarrow 0$ *after* the lift-up.

Since the lift-ups have been completed in the previous subsection, all that is left is letting $s \rightarrow 0$. Suppose the limit is taken in a chart. As seen in the previous subsection, some of the lift-ups of \mathcal{C} 's and/or δ 's may be invisible; that is, the limit consists only of the components visible in that chart. Thus the limit should be taken in every chart and the final form of $\lim_{s \rightarrow 0} \mathcal{C}$ is obtained as their union.

In chart 1 and chart 2, we can see from (3.20), (3.21) and (3.23) that $\lim_{s \rightarrow 0} \mathcal{C}_i = \delta_i$ for $i = p_0, p_1$. In chart 3, we encounter the first nontrivial result. From (3.24), we find in chart 3_{zxx} as

$$\lim_{s \rightarrow 0} \mathcal{C}_{p_0} = \delta_{p_0}, \quad \lim_{s \rightarrow 0} \mathcal{C}_{p_2} = \{\tilde{x}_1 = 0, y_3^2 = 0\} = 2\delta_{p_2}. \quad (3.34)$$

\mathcal{C}_{p_2} has only one component for $s \neq 0$, but after $s \rightarrow 0$, it splits into two overlapping (multiplicity two) δ_{p_2} 's. Similarly, from (3.26), we find in chart 3_{zxx} as

$$\lim_{s \rightarrow 0} \mathcal{C}_{p_1} = \delta_{p_1}, \quad \lim_{s \rightarrow 0} \mathcal{C}_{p_2} = \{z_2 = 0, y_3^2 = 0\} = 2\delta_{p_2}. \quad (3.35)$$

In chart 3_{zxy} , $\lim_{s \rightarrow 0} \mathcal{C}_{p_2}$ is invisible.

Next we consider charts 4_{zx*x} arising from the blow-up of q_1 . In chart 4_{zx*x} , \mathcal{C}_{p_2} is visible, but δ_{p_2} is invisible (see (3.28)). Nevertheless, $\lim_{s \rightarrow 0} \mathcal{C}_{p_2}$ does exist. Actually, one can see from (3.28) that

$$\lim_{s \rightarrow 0} \mathcal{C}_{p_2} = \delta_{q_1}. \quad (3.36)$$

Also, we find $\lim_{s \rightarrow 0} \mathcal{C}_{p_0} = \delta_{p_0}$, $\lim_{s \rightarrow 0} \mathcal{C}_{q_1} = \delta_{q_1}$. One can show that the same results are obtained in chart 4_{zxxy} except that \mathcal{C}_{p_0} is invisible. In chart 4_{zx*xz} , one can see from (3.32) that \mathcal{C}_{p_2} splits into two components as follows:

$$\begin{aligned} \lim_{s \rightarrow 0} \mathcal{C}_{p_2} &= \{x_4 z_3 = 0, y_4^2 = x_4\} \\ &= \{x_4 = 0, y_4^2 = 0\} \cup \{z_3 = 0, y_4^2 = x_4\} \\ &= 2\delta_{p_2} + \delta_{q_1}. \end{aligned} \quad (3.37)$$

Also, $\lim_{s \rightarrow 0} \mathcal{C}_{q_1} = \delta_{q_1}$ is satisfied.

In charts 4_{zxz*} , which arise from the blow-up of r_2 , one can show by repeating the same argument that

$$\begin{aligned} \lim_{s \rightarrow 0} \mathcal{C}_{p_2} &= 2\delta_{p_2} + \delta_{r_2} \quad (\text{chart } 4_{zxzx}), \\ \lim_{s \rightarrow 0} \mathcal{C}_{p_2} &= \delta_{r_2}, \quad (\text{chart } 4_{zxzy}, 4_{zxzz}). \end{aligned} \quad (3.38)$$

All the other curves satisfy $\lim_{s \rightarrow 0} \mathcal{C}_i = \delta_i$.

Finally, after blowing up q_2 , charts 3_{zz*} contain \mathcal{C}_{q_2} as well as the lift-ups of \mathcal{C}_{p_0} and \mathcal{C}_{p_1} . A similar analysis shows that $\lim_{s \rightarrow 0} \mathcal{C}_i = \delta_i$ for $i = p_0, p_1$ and q_2 .

Collecting all the above results, we find only \mathcal{C}_{p_2} has a non-trivial limit. The final form of $\lim_{s \rightarrow 0} \mathcal{C}_{p_2}$ is given by the union of the components that are visible in each chart, and hence from (3.34), (3.35), (3.36), (3.37) and (3.38),

$$\lim_{s \rightarrow 0} \mathcal{C}_{p_2} = 2\delta_{p_2} + \delta_{q_1} + \delta_{r_2}. \quad (3.39)$$

In conclusion, we find (Hereafter, $\lim_{s \rightarrow 0}$ will be omitted.)

$$\begin{aligned} \mathcal{C}_{p_0} &= \delta_{p_0}, \\ \mathcal{C}_{p_1} &= \delta_{p_1}, \\ \mathcal{C}_{p_2} &= 2\delta_{p_2} + \delta_{q_1} + \delta_{r_2}, \\ \mathcal{C}_{q_1} &= \delta_{q_1}, \\ \mathcal{C}_{r_2} &= \delta_{r_2}, \\ \mathcal{C}_{q_2} &= \delta_{q_2}. \end{aligned} \quad (3.40)$$

The intersection matrix of \mathcal{C} 's is the minus of the $D_6 = SO(12)$ Cartan matrix:

$$-\mathcal{C}_I \cdot \mathcal{C}_J = \begin{pmatrix} 2 & -1 & 0 & 0 & 0 & 0 \\ -1 & 2 & -1 & 0 & 0 & 0 \\ 0 & -1 & 2 & -1 & 0 & 0 \\ 0 & 0 & -1 & 2 & -1 & -1 \\ 0 & 0 & 0 & -1 & 2 & 0 \\ 0 & 0 & 0 & -1 & 0 & 2 \end{pmatrix}, \quad (3.41)$$

where $I, J = q_1, p_0, p_2, p_1, r_2, q_2$ in this order. Note that this is different from the order of the blow-ups (see the upper rightmost diagram in Figure 1, or equivalently, the upper diagram in Figure 2 below). From (3.40), δ 's are expressed in terms of \mathcal{C} 's. Then one can compute the intersection matrix of δ 's, which is found to be

$$-\delta_I \cdot \delta_J = \begin{pmatrix} 2 & -1 & -1 & 0 & 0 & 0 \\ -1 & 2 & 0 & 0 & 0 & 0 \\ -1 & 0 & \frac{3}{2} & 0 & -1 & 0 \\ 0 & 0 & 0 & 2 & -1 & -1 \\ 0 & 0 & -1 & -1 & 2 & 0 \\ 0 & 0 & 0 & -1 & 0 & 2 \end{pmatrix}. \quad (3.42)$$

This is the minus of the $A_6 = SU(7)$ Cartan matrix, except that the self-intersection number of δ_{p_2} is not -2 , but $-\frac{3}{2}$. Namely, it is true that the intersection pattern of δ 's is given by the A_6 Dynkin diagram, but their intersection “numbers” are slightly different from the corresponding A_6 Cartan matrix. This difference is expressed in the lower diagram in Figure 2 as the triangular (not circular) node. In summary,

$$\begin{aligned} \text{intersection pattern} &\Rightarrow A_6 \text{ Dynkin diagram,} \\ \text{intersection numbers} &\Rightarrow A_6 \text{ Dynkin diagram with a triangular node.} \end{aligned} \quad (3.43)$$

Let us call the latter diagram “intersection diagram”. Since it contains a $-\frac{3}{2}$ node, it is *not* a usual A_6 Dynkin diagram. In this sense, we conclude in the present case that the intersection diagram is an A_6 “non-Dynkin” diagram.

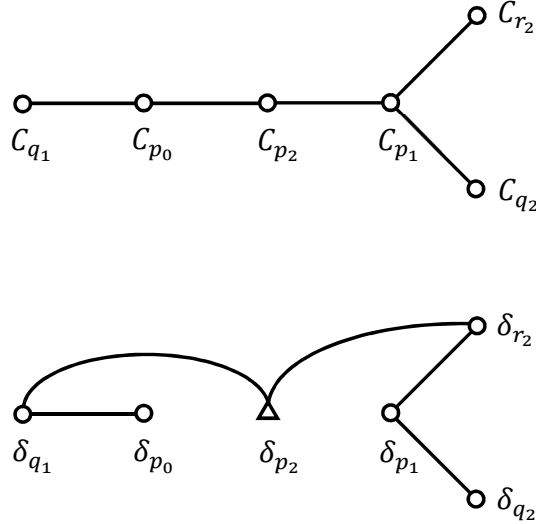


Figure 2. Generic $SO(12)$ intersection diagram at $s \neq 0$ (upper) and incomplete intersection diagram at $s = 0$ (lower) of $SO(12) \rightarrow E_7 : p_1$ -first ($p_0 \rightarrow p_1 \rightarrow p_2$) case.

In terms of \mathcal{C} 's, δ_{p_2} is written as $\delta_{p_2} = \frac{1}{2}(\mathcal{C}_{p_2} - \mathcal{C}_{q_1} - \mathcal{C}_{r_2})$. This is one of the weights in the spinor representation of $SO(12)$. Thus we see that at a generic $s \neq 0$ codimension-one

locus of the singularity the exceptional fibers after the resolutions form a root system of $SO(12)$, but at $s = 0$ one of the simple roots (\mathcal{C}_{p_2}) is transmuted to a weight in the spinor representation (δ_{p_2}).

These δ 's form a basis of the two-cycles appearing at the codimension-two singularity after the resolution. Let us consider the lattice spanned by δ 's :

$$J = \sum_{I=q_1, p_0, p_2, p_1, r_2, q_2} n_I \delta_I \quad (n_I \in \mathbb{Z}), \quad (3.44)$$

where each lattice point expresses a two-cycle at $s = 0$. One can show by using (3.42) that

$$\begin{aligned} \#(J \cdot J = -2) &= 60, \\ \#(J \cdot J = -\frac{3}{2}) &= 32. \end{aligned} \quad (3.45)$$

They respectively correspond to the adjoint representation (except the Cartan part) of $SO(12)$ and the spinor representation $\mathbf{32}$ of $SO(12)$. The latter representation consists of 16 states with $n_I \geq 0$ for all I and 16 states with $n_I \leq 0$ for all I . Note that, unlike in the cases of the ordinary (the complete) resolutions (1.1), there appears only *one* irreducible representation (= $\mathbf{32}$) in the integer span of the two-cycles at the singularity, indicating that it is a half-hypermultiplet.

3.2 Complete resolution: Blowing up p_1 first

3.2.1 Blowing up process

The geometry of complete resolution is given by setting $H_{n-r+4} = s^2$ instead of $H_{n-r+4} = s$ in (2.13) and (2.14) (the other polynomials are unchanged), we have

$$\Phi(x, y, z, s) = -y^2 + x^3 + f(z, s)x + g(z, s) = 0, \quad (3.46)$$

where

$$\begin{aligned} f(z, s) &= -3s^4 z^2 + z^3, \\ g(z, s) &= 2s^6 z^3 - s^2 z^4. \end{aligned} \quad (3.47)$$

Singularities can be blown up in the same way as in section 3.1.1. As a result, a new isolated (codimension-two) singularity p_3 arises in chart 3 after p_2 is blown up in chart 2_{zx} . Regarding the structure of singularities, this is the only difference between complete and incomplete cases (see Table 2 below).

Explicitly, the 3rd blow up (3.10) and (3.11) are replaced as follows:

3rd blow up

Chart 3_{zxx}

$$\begin{aligned} \Psi_{zx}(\tilde{x}_1, \tilde{x}_1 y_3, \tilde{x}_1 z_3, s) &= \tilde{x}_1^2 \Psi_{zxx}(\tilde{x}_1, y_3, z_3, s), \\ \Psi_{zxx}(\tilde{x}_1, y_3, z_3, s) &= z_3(3s^2 + \tilde{x}_1 z_3 + \tilde{x}_1) - y_3^2, \\ \mathcal{C}_{p_2} \text{ in } 3_{zxx} &: \tilde{x}_1 = 0, \quad y_3^2 = 3s^2 z_3. \\ \text{Singularities} &: (\tilde{x}_1, y_3, z_3, s) = (-3s^2, 0, 0, s)(= q_1), (0, 0, -1, 0)(= p_3). \end{aligned} \quad (3.48)$$

Table 2. $SO(12) \rightarrow E_7$: Complete case when p_1 is blown up first ($p_0 \rightarrow p_1 \rightarrow p_2$). The new isolated codimension-two conifold singularity is shown in red.

	1st blow up	2nd blow up	3rd blow up	4th blow up
$\mathcal{Q}_0 \rightarrow$	$\mathcal{Q}_1(s^2 : 0 : 1) \rightarrow$ $q_1(-2s^2 : 0 : 1)$	$\mathcal{Q}_2(1 : 0 : 0)$ (in 2_{zx}) \rightarrow $q_1(1 : 0 : 0)(\tilde{x}_1 = -3s^2)$ $r_2(1 : 0 : -3s^2)$ $\mathcal{Q}_2(0 : 0 : 1)$ (in 2_{zz}) \rightarrow	$\mathcal{Q}_3(1 : 0 : 0; s = 0)$ (codim.2) \rightarrow $\mathcal{Q}_1(1 : 0 : 0)(\tilde{x}_1 = -3s^2) \rightarrow$ $\mathcal{Q}_2(0 : 0 : 1)(z_2 = -3s^2) \rightarrow$ regular	regular regular regular

Chart 3_{xy} Regular.

Chart 3_{xz}

$$\begin{aligned}\Psi_{zx}(x_3 z_2, y_3 z_2, z_2, s) &= z_2^2 \Psi_{zxx}(x_3, y_3, z_2, s), \\ \Psi_{zxx}(x_3, y_3, z_2, s) &= 3s^2 x_3 + x_3(x_3 + 1)z_2 - y_3^2. \\ \mathcal{C}_{p_2} \text{ in } 3_{zxz} &: z_2 = 0, \quad y_3^2 = 3s^2 x_3. \\ \text{Singularities} &: (x_3, y_3, z_2, s) = (0, 0, -3s^2, s) (= r_2), (-1, 0, 0, 0) (= p_3).\end{aligned}\quad (3.49)$$

The new isolated singularity p_3 is the conifold singularity. To see this, consider chart 3_{zxx} (3.48) and shift p_3 to the origin via

$$\tilde{z}_3 \equiv z_3 + 1. \quad (3.50)$$

The defining equation then reads

$$\Upsilon_{zxx}(\tilde{x}_1, y_3, \tilde{z}_3, s) \equiv \Psi_{zxx}(\tilde{x}_1, y_3, \tilde{z}_3 - 1, s). \quad (3.51)$$

The explicit form is

$$\Upsilon_{zxx}(\tilde{x}_1, y_3, \tilde{z}_3, s) = -y_3^2 + (-1 + \tilde{z}_3)(\tilde{x}_1 \tilde{z}_3 + 3s^2), \quad (3.52)$$

where p_3 is located at $(\tilde{x}_1, y_3, \tilde{z}_3, s) = (0, 0, 0, 0)$. The leading terms of Υ_{zxx} can be written as $\Upsilon_{zxx} \sim \tilde{z}_3(-\tilde{x}_1) - (y_3 + i\sqrt{3}s)(y_3 - i\sqrt{3}s) \sim X_1 X_4 - X_2 X_3$, and hence $\Upsilon_{zxx} = 0$ is a conifold. Including the subleading terms, we have

$$\begin{aligned}\Upsilon_{zxx}(\tilde{x}_1, y_3, \tilde{z}_3, s) &= \tilde{z}_3(-\tilde{x}_1 + \tilde{x}_1 \tilde{z}_3 + 3s^2) - (y_3 + i\sqrt{3}s)(y_3 - i\sqrt{3}s) \\ &= X_1 X_4 - X_2 X_3,\end{aligned}\quad (3.53)$$

where X_i are given by ⁵

$$\begin{aligned}X_1 &= \tilde{z}_3, \\ X_4 &= -\tilde{x}_1 + \tilde{x}_1 \tilde{z}_3 + 3s^2, \\ X_2 &= y_3 + i\sqrt{3}s, \\ X_3 &= y_3 - i\sqrt{3}s.\end{aligned}\quad (3.54)$$

⁵ One may exchange the definitions of X_1 and X_4 , or X_2 and X_3 , but it does not change the result ((3.65) below). It also holds for all the other cases discussed in this paper.

p_3 is located at the origin $(X_1, X_2, X_3, X_4) = (0, 0, 0, 0)$, which is the conifold singularity.

The exceptional curves existing in chart 3_{zxx} are given by replacing s to s^2 in (3.24). After the coordinate changes (3.50) and (3.54), their positions read

Chart 3_{zxx}

$$\begin{aligned} \mathcal{C}_{p_2} : X_4 &= -3s^2, \frac{(X_2 + X_3)^2}{4} = 3s^2(X_1 - 1), \quad \delta_{p_2} : X_4 = 0, X_2 = X_3 = 0, \\ \mathcal{C}_{p_1} : &\text{Invisible} \quad \quad \quad \delta_{p_1} : \text{Invisible}, \\ \mathcal{C}_{p_0} : X_1 &= 1, X_2 + X_3 = 0 \quad \quad \quad \delta_{p_0} : X_1 = 1, X_2 = X_3 = 0, \end{aligned} \quad (3.55)$$

where $s = -\frac{i}{2\sqrt{3}}(X_2 - X_3)$. The conifold singularity p_3 is contained in δ_{p_2} , but not in δ_{p_0} . Similarly, in chart 3_{zzz} , p_3 is on δ_{p_2} , but not on δ_{p_1} . As for Figure 1, one new point p_3 is added on δ_{p_2} in the second figure of the bottom line.

3.2.2 Intersection diagram at $s = 0$

Since p_3 is a codimension-two singularity, it does not change the intersection diagram for generic $s \neq 0$ (ordinary $SO(12)$ Dynkin diagram in Figure 2). Here we examine how the intersection diagram at $s = 0$ is modified via the resolution of p_3 .

The conifold singularity p_3 is resolved by inserting an exceptional curve \mathbb{P}^1 at the origin. This process is called the small resolution. We write the inserted \mathbb{P}^1 as δ_{complete} . Since p_3 is contained only in δ_{p_2} , δ_{complete} intersects only with δ_{p_2} . Adding this node to Figure 2, we find that the intersection pattern becomes E_7 (see Figure 3 below). At this stage, however, it is not clear what intersection matrix is associated with this diagram. To clarify it, we need a lift-up.

The smooth geometry after the small resolution is covered by two local coordinate patches H_+ and H_- (see Appendix C). By lifting up the relevant objects from chart 3 into these patches, one can examine how the limit $s \rightarrow 0$ is modified from the incomplete case and what intersection matrix is obtained. Since p_3 is separated from δ_{p_0} and δ_{p_1} , lifting up \mathcal{C}_{p_2} and δ_{p_2} is sufficient. We consider chart 3_{zxx} (3.55).

The local coordinates of H_+ are (X'_2, X'_4, λ) and the resolved geometry is obtained by the replacement (C.4):

$$(X_1, X_2, X_3, X_4) = (-\lambda X'_2, X'_2, -\lambda X'_4, X'_4). \quad (3.56)$$

Here we put ' for the coordinates after the small resolution. The explicit form of δ_{complete} in chart H_+ is given by (C.5). The lift-ups of \mathcal{C}_{p_2} and δ_{p_2} are given by substituting (3.56) into (3.55). Then we have

Chart H_+

$$\begin{aligned} \delta_{\text{complete}} : (X'_2, X'_4, \lambda) &= (0, 0, \lambda), \\ \mathcal{C}_{p_2} : X'_4 &= -3s^2, \frac{(X'_2 - \lambda X'_4)^2}{4} = 3s^2(-\lambda X'_2 - 1), \quad \delta_{p_2} : \text{Invisible}, \end{aligned} \quad (3.57)$$

where

$$s = -\frac{i}{2\sqrt{3}}(X'_2 + \lambda X'_4). \quad (3.58)$$

δ_{p_2} is invisible, since δ_{p_2} (3.55) is given by $(-\lambda X'_2, X'_2, -\lambda X'_4, X'_4) = (X_1, 0, 0, 0)$ with $X_1 \neq 0$, which is impossible. In this patch, δ_{p_2} and δ_{complete} do not intersect. The $s \rightarrow 0$ limit is given by the replacement $X'_2 = -\lambda X'_4$, and hence

$$\begin{aligned} \lim_{s \rightarrow 0} \mathcal{C}_{p_2} &= \{X'_4 = 0, \lambda^2 X_4'^2 = 0\} \quad \text{with } X'_2 = -\lambda X'_4 \\ &= \{(X'_2, X'_4, \lambda) = (0, 0, \lambda)\} \\ &= \delta_{\text{complete}}. \end{aligned} \quad (3.59)$$

In the other patch H_- , the local coordinates are (X'_1, X'_3, μ) and the resolution is given by (C.7):

$$(X_1, X_2, X_3, X_4) = (X'_1, -\mu X'_1, X'_3, -\mu X'_3). \quad (3.60)$$

In this patch, δ_{complete} (C.8) as well as \mathcal{C}_{p_2} and δ_{p_2} (3.55) take the following forms:

Chart H_-

$$\begin{aligned} \delta_{\text{complete}} &: (X'_1, X'_3, \mu) = (0, 0, \mu), \\ \mathcal{C}_{p_2} : \mu X'_3 &= 3s^2, \frac{(X'_3 - \mu X'_1)^2}{4} = 3s^2(X'_1 - 1), \delta_{p_2} : (X'_1, X'_3, \mu) = (X'_1, 0, 0), \end{aligned} \quad (3.61)$$

where

$$s = \frac{i}{2\sqrt{3}}(X'_3 + \mu X'_1). \quad (3.62)$$

This time, δ_{p_2} is visible. δ_{p_2} and δ_{complete} are intersecting at $(X'_1, X'_3, \mu) = (0, 0, 0)$:

$$\delta_{p_2} \cdot \delta_{\text{complete}} \neq 0. \quad (3.63)$$

The $s \rightarrow 0$ limit is given by the replacement $X'_3 = -\mu X'_1$:

$$\begin{aligned} \lim_{s \rightarrow 0} \mathcal{C}_{p_2} &= \{-\mu^2 X'_1 = 0, \mu^2 X_1'^2 = 0\} \quad \text{with } X'_3 = -\mu X'_1 \\ &= \{X'_1 = 0\} \cup \{\mu^2 = 0\} \quad \text{with } X'_3 = -\mu X'_1 \\ &= \{(X'_1, X'_3, \mu) = (0, 0, \mu)\} \cup \{(X'_1, X'_3, \mu) = (X'_1, 0, 0)\}^{\otimes 2} \\ &= \delta_{\text{complete}} + 2\delta_{p_2}. \end{aligned} \quad (3.64)$$

In conclusion, for the complete resolution, the new exceptional curve δ_{complete} is contained in $\lim_{s \rightarrow 0} \mathcal{C}_{p_2}$ with multiplicity one, and (3.40) is modified as

$$\begin{aligned} \mathcal{C}_{p_0} &= \delta_{p_0}, \\ \mathcal{C}_{p_1} &= \delta_{p_1}, \\ \mathcal{C}_{p_2} &= 2\delta_{p_2} + \delta_{q_1} + \delta_{r_2} + \delta_{\text{complete}}, \\ \mathcal{C}_{q_1} &= \delta_{q_1}, \\ \mathcal{C}_{r_2} &= \delta_{r_2}, \\ \mathcal{C}_{q_2} &= \delta_{q_2}. \end{aligned} \quad (3.65)$$

Then, assuming that the intersection matrix of these seven δ 's is just the minus of ordinary E_7 Cartan matrix, we find that the intersection matrix of the six \mathcal{C} 's computed by (3.65) is

precisely the minus of the $SO(12)$ Cartan matrix. It means that, in contrast to the incomplete case, δ 's have no node with self-intersection number $-\frac{3}{2}$ and the intersection diagram is the ordinary E_7 Dynkin diagram. That is, δ_{p_2} , whose self-intersection number is $-\frac{3}{2}$ (triangular node) in the incomplete case, becomes the ordinary node with self-intersection -2 (circular node) by virtue of the existence of δ_{complete} . The result is summarized in Figure 3. As usual, two cycles J spanned by the seven δ 's with $J \cdot J = -2$ contain two **32**'s as in (1.1).

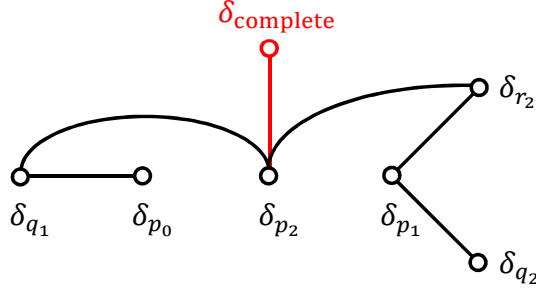


Figure 3. Complete E_7 intersection diagram of $SO(12) \rightarrow E_7 : p_1$ -first ($p_0 \rightarrow p_1 \rightarrow p_2$) case.

3.3 Incomplete resolution: Blowing up q_1 first

3.3.1 Blowing up process

In section 3.1, between the two singularities p_1 and q_1 arising from the first blow up in chart 1_z (3.6), p_1 was blown up first. In this section, let us blow up q_1 first and see the differences. This time we make a shift of the coordinate x_1 so that q_1 comes to $(0, 0, 0, s)$: We define

$$\Sigma_z(\tilde{x}_1, y_1, z, s) \equiv \Phi_z(\tilde{x}_1 - 2s, y_1, z, s). \quad (3.66)$$

$\Sigma_z(\tilde{x}_1, y_1, z, s) = 0$ has singularities $(3s, 0, 0, s)$ ($= p_1$) and $(0, 0, 0, s)$ ($= q_1$). We blow up the latter singularity. The process is completely parallel to that in the previous section so we will only describe the relevant charts and show the main differences from the previous case. For later use, we also present the definition of δ and the lift-ups of \mathcal{C} and δ . For the p_1 -first case studied in the previous sections, the exceptional curves arising from the blow-ups of the singularities p_0, p_1, p_2, q_1, r_2 and q_2 are respectively expressed by $\mathcal{C}_{p_0}, \mathcal{C}_{p_1}, \mathcal{C}_{p_2}, \mathcal{C}_{q_1}, \mathcal{C}_{r_2}$ and \mathcal{C}_{q_2} . We use the same notation for the q_1 -first case as well.

2nd blow up From the blow-up of q_1 , \mathcal{C}_{q_1} arises. \mathcal{C}_{p_0} and δ_{p_0} are lifted up from chart 1_z .

Chart 2_{zx}

$$\begin{aligned}
\Sigma_z(\tilde{x}_1, \tilde{x}_1 y_2, \tilde{x}_1 z_2, s) &= \tilde{x}_1^2 \Sigma_{zx}(\tilde{x}_1, y_2, z_2, s), \\
\Sigma_{zx}(\tilde{x}_1, y_2, z_2, s) &= z_2(3s - \tilde{x}_1)(3s - \tilde{x}_1 - z_2) - y_2^2. \\
\mathcal{C}_{q_1} : \tilde{x}_1 &= 0, \quad 3s z_2(3s - z_2) - y_2^2 = 0, & \delta_{q_1} : \tilde{x}_1 &= 0, \quad y_2 = 0, \\
\mathcal{C}_{p_0} : z_2 &= 0, \quad y_2 = 0 & , & \delta_{p_0} : z_2 = 0, \quad y_2 = 0. \\
\text{Singularities} : (\tilde{x}_1, y_2, z_2, s) &= (3s, 0, 0, s)(= p_1). & & (3.67)
\end{aligned}$$

The positions of these objects are depicted in the leftmost column of Figure 4. There are no other singularities in chart 2_{zy} or 2_{zz} , so we blow up p_1 in chart 2_{zx} . Again, we need to shift the coordinate so that the singularity we now blow up comes to the origin:

$$\Psi_{zx}(\tilde{\tilde{x}}_1, y_2, z_2, s) \equiv \Sigma_{zx}(\tilde{\tilde{x}}_1 + 3s, y_2, z_2, s). \quad (3.68)$$

3rd blow up The relevant charts are 3_{zxx} and 3_{zxx} . From the blow-up of p_1 , \mathcal{C}_{p_1} arises.

Chart 3_{zxx}

$$\begin{aligned}
\Psi_{zx}(\tilde{\tilde{x}}_1, \tilde{\tilde{x}}_1 y_3, \tilde{\tilde{x}}_1 z_3, s) &= \tilde{\tilde{x}}_1^2 \Psi_{zxx}(\tilde{\tilde{x}}_1, y_3, z_3, s), \\
\Psi_{zxx}(\tilde{\tilde{x}}_1, y_3, z_3, s) &= \tilde{\tilde{x}}_1 z_3(z_3 + 1) - y_3^2. \\
\mathcal{C}_{p_1} : \tilde{\tilde{x}}_1 &= 0, \quad y_3 = 0 & , & \delta_{p_1} : \tilde{\tilde{x}}_1 &= 0, \quad y_3 = 0, \\
\mathcal{C}_{q_1} : \tilde{\tilde{x}}_1 &= -3s, \quad \tilde{\tilde{x}}_1 z_3(1 + z_3) - y_3^2 = 0, & \delta_{q_1} : & \text{Invisible}, \\
\mathcal{C}_{p_0} : z_3 &= 0, \quad y_3 = 0 & , & \delta_{p_0} : z_3 = 0, \quad y_3 = 0. \\
\text{Singularities} : (\tilde{\tilde{x}}_1, y_3, z_3, s) &= (0, 0, -1, s)(= r_2), (0, 0, 0, s)(= p_2). & & (3.69)
\end{aligned}$$

Chart 3_{zxz}

$$\begin{aligned}
\Psi_{zx}(x_3 z_2, y_3 z_2, z_2, s) &= z_2^2 \Psi_{zxz}(x_3, y_3, z_2, s), \\
\Psi_{zxz}(x_3, y_3, z_2, s) &= x_3(x_3 + 1)z_2 - y_3^2. \\
\mathcal{C}_{p_1} : z_2 &= 0, \quad y_3 = 0 & , & \delta_{p_1} : z_2 = 0, \quad y_3 = 0, \\
\mathcal{C}_{q_1} : x_3 z_2 &= -3s, \quad x_3 z_2(x_3 + 1) - y_3^2 = 0, & \delta_{q_1} : & x_3 = 0, \quad y_3 = 0, \\
\mathcal{C}_{p_0} : & \text{Invisible} & , & \delta_{p_0} : \text{Invisible}. \\
\text{Singularities} : (x_3, y_3, z_2, s) &= (-1, 0, 0, s)(= r_2), (0, 0, 0, s)(= q_2). & & (3.70)
\end{aligned}$$

Note that \mathcal{C}_{q_1} and δ_{q_1} are independently lifted up from (3.67). The positions of these objects are depicted in the middle column of Figure 4. One can see from (3.69) and (3.70) that the remaining three singularities p_2 , r_2 and q_2 are separated for all s (not only for $s \neq 0$ but also for $s = 0$), and hence they are independently blown up. The whole blowing up process is summarized in Table 3. The resulting intersection patterns are depicted in the rightmost column of Figure 4. For $s \neq 0$, the intersection pattern is the D_6 Dynkin diagram, which is identical to the one in the p_1 -first case (see the upper rightmost diagram in Figure 1, or the upper diagram in Figure 2). The orders of the nodes are the same as well. On the other hand, the intersection pattern at $s = 0$ is the E_6 Dynkin diagram, which is different from the one (A_6) in the p_1 -first case.

Table 3. $SO(12) \rightarrow E_7$: Incomplete case when q_1 is blown up first ($p_0 \rightarrow q_1$).

	1st blow up	2nd blow up	3rd blow up	4th blow up
$\mathbb{Q}_0 \rightarrow$	$\mathbb{Q}_1(-2s : 0 : 1) \rightarrow$ $p_1(s : 0 : 1)$	regular $\mathbb{Q}_1(1 : 0 : 0)(\tilde{x}_1 = 3s) \rightarrow$	$\mathbb{P}_2(1 : 0 : 0) \rightarrow$ $\mathbb{Q}_2(0 : 0 : 1) \rightarrow$ $\mathbb{Q}_2(1 : 0 : -1) \rightarrow$	regular regular regular

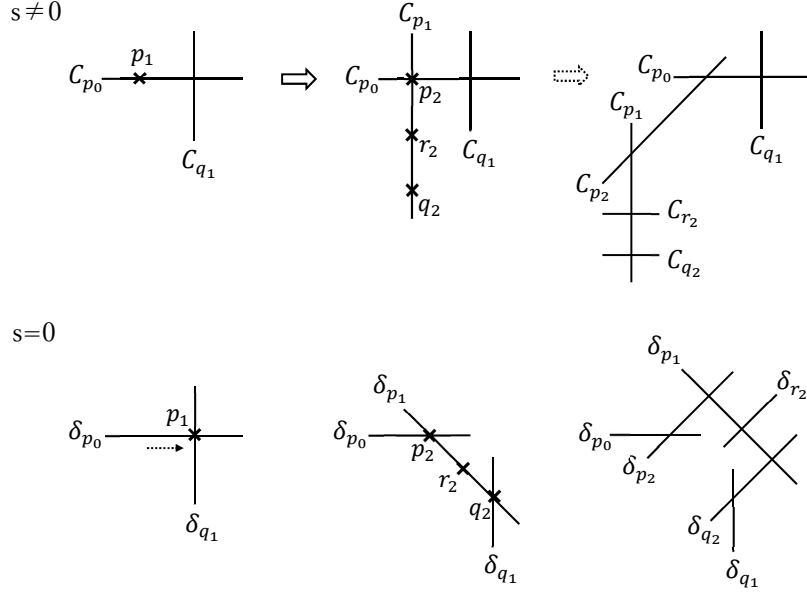


Figure 4. Exceptional curves and singularities of $SO(12) \rightarrow E_7 : p_0 \rightarrow q_1$ case.

3.3.2 Intersection diagram at $s = 0$: Differences from the p_1 -first case

Following the same procedure given in section 3.1.3, we find the $s \rightarrow 0$ limit of \mathcal{C} for the q_1 -first case as

$$\begin{aligned}
 \mathcal{C}_{p_0} &= \delta_{p_0}, \\
 \mathcal{C}_{q_1} &= 2\delta_{q_1} + 2\delta_{p_1} + \delta_{p_2} + 2\delta_{q_2} + \delta_{r_2}, \\
 \mathcal{C}_{p_1} &= \delta_{p_1}, \\
 \mathcal{C}_{p_2} &= \delta_{p_2}, \\
 \mathcal{C}_{r_2} &= \delta_{r_2}, \\
 \mathcal{C}_{q_2} &= \delta_{q_2}.
 \end{aligned} \tag{3.71}$$

The first two terms of \mathcal{C}_{q_1} are readily observed in chart 3 (see (3.69) and (3.70)). The other terms of \mathcal{C}_{q_1} can only be seen in deeper charts. We skip the detail of the derivation.

The intersection matrix among \mathcal{C} 's is the same one with the p_1 -first case and is given by (3.41) with the same order $I, J = q_1, p_0, p_2, p_1, r_2, q_2$. Then (3.71) yields the intersection matrix of δ 's as

$$-\delta_I \cdot \delta_J = \begin{pmatrix} \frac{3}{2} & 0 & 0 & 0 & 0 & -1 \\ 0 & 2 & -1 & 0 & 0 & 0 \\ 0 & -1 & 2 & -1 & 0 & 0 \\ 0 & 0 & -1 & 2 & -1 & -1 \\ 0 & 0 & 0 & -1 & 2 & 0 \\ -1 & 0 & 0 & -1 & 0 & 2 \end{pmatrix}. \quad (3.72)$$

This is almost the E_6 Cartan matrix except that the self-intersection number of δ_{q_1} is $-\frac{3}{2}$, which is expressed as a triangular node in Figure 5. Thus the intersection diagram for this case is an E_6 non-Dynkin diagram.

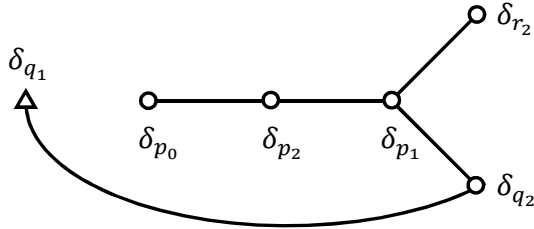


Figure 5. Incomplete intersection diagram of $SO(12) \rightarrow E_7 : q_1$ -first ($p_0 \rightarrow q_1$) case.

We can search for the elements of the form $\sum_{I=q_1, p_0, p_2, p_1, r_2, q_2} n_I \delta_I$ whose square is $-\frac{3}{2}$ to find, again, that there are $16 + 16$ such elements, the former of which have $n_I \geq 0$ for all I , and the latter of which have $n_I \leq 0$ for all I . Thus, in this case as well, there is only *one* irreducible representation ($= \mathbf{32}$) at the singularity, showing that it is a half-hypermultiplet.

3.4 Complete resolutions: Blowing up q_1 first

The process of the blow-ups is almost the same as that in the incomplete resolutions. A difference arises in chart 2_{zz} , where a conifold singularity is developed at $(x_2, y_2, z, s) = (0, 0, 0, 0)$, which we denote by q_3 (shown in red in Table 4), where the relation to the coordinates in chart 1_z is $(\tilde{x}_1, y_1, z, s) = (x_2 z, y_2 z, z, s)$. This is an isolated codimension-two singularity developed only at $s = 0$. Since this is in chart 2_{zz} , this singularity is located at $(0 : 0 : 1)$ on \mathbb{P}^2 emerged by the blow up at $s = 0$. Therefore, it is not visible in chart 2_{zx} or 3_{zx^*} . Moreover, after the coordinate shift similar to (3.66), Ψ_{zx} becomes identical to the incomplete case. Thus the process is the same as the incomplete case afterwards. Therefore, the only extra exceptional curve is the one arising from the small resolution of the isolated conifold singularity on δ_{q_1} . This adds an extra node to the diagram in the Figure 5, as we show in Figure 6. We denote this new curve as δ_{complete} here. This is E_7 , and the extra node again extends from δ_{q_1} that was the “weight” node represented by the triangle in the incomplete case. How δ_{complete} modifies the $\lim_{s \rightarrow 0} \mathcal{C}$ can be seen in the same

way as explained in section 3.2.2. The result is

$$\begin{aligned}
\mathcal{C}_{p_0} &= \delta_{p_0}, \\
\mathcal{C}_{q_1} &= 2\delta_{q_1} + 2\delta_{p_1} + \delta_{p_2} + 2\delta_{q_2} + \delta_{r_2} + \delta_{\text{complete}}, \\
\mathcal{C}_{p_1} &= \delta_{p_1}, \\
\mathcal{C}_{p_2} &= \delta_{p_2}, \\
\mathcal{C}_{r_2} &= \delta_{r_2}, \\
\mathcal{C}_{q_2} &= \delta_{q_2}.
\end{aligned} \tag{3.73}$$

This reproduces the minus of the D_6 Cartan matrix as the intersection matrix of \mathcal{C} 's if the intersections among δ 's are given by the minus of the proper E_7 Cartan matrix. Therefore, in the complete case, δ_{q_1} becomes an ordinary node with self-intersection -2 as shown in Figure 6.

Table 4. $SO(12) \rightarrow E_7$: Complete case when q_1 is blown up first ($p_0 \rightarrow q_1$).

	1st blow up	2nd blow up	3rd blow up	4th blow up
$\mathcal{P}_0 \rightarrow$	$\mathcal{Q}_1(-2s : 0 : 1) \rightarrow$ $p_1(s : 0 : 1)$	$\mathcal{Q}_3(0 : 0 : 1; s = 0)(\text{codim.2}) \rightarrow$ $\mathcal{Q}_1(1 : 0 : 0)(\tilde{x}_1 = 3s) \rightarrow$	regular $\mathcal{Q}_2(1 : 0 : 0) \rightarrow$ $\mathcal{Q}_2(0 : 0 : 1) \rightarrow$ $\mathcal{Q}_2(1 : 0 : -1) \rightarrow$	regular regular regular

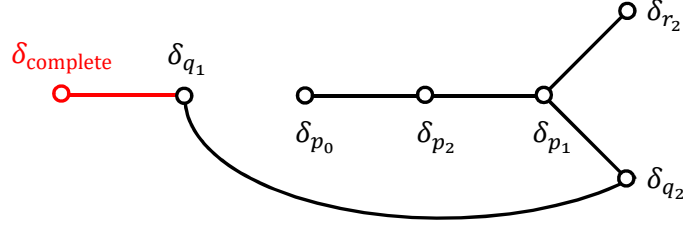


Figure 6. Complete E_7 intersection diagram of $SO(12) \rightarrow E_7$: q_1 -first ($p_0 \rightarrow q_1$) case.

3.5 Other inequivalent orderings

So far we have considered incomplete and complete resolutions where the order of blowing up singularities is $p_0 \rightarrow p_1 \rightarrow p_2$ and $p_0 \rightarrow q_1$. In the former case, we have also two codimension-one singularities q_1 and r_2 , besides p_2 and q_2 , after the 2nd blow up, as shown in Table 1. Since q_2 never coincides with the other three for any value of s , it can be blown up independently at any stage. On the other hand, p_2 , q_1 and r_2 become the same point $(1 : 0 : 0)$ on the \mathbb{P}^2 at $s = 0$, so a different intersection diagram arises if we blow up q_1 or

r_2 instead of p_2 after blowing up p_1 . The concrete process is similar to the previous cases so we only describe the results.

$p_0 \rightarrow p_1 \rightarrow q_1$ case

If q_1 is blown up after p_1 , the relations among \mathcal{C} 's and δ 's are given by (the modifications via δ_{complete} in the complete case are shown in the parentheses)

$$\begin{aligned}
\mathcal{C}_{p_0} &= \delta_{p_0}, \\
\mathcal{C}_{p_1} &= \delta_{p_1} + \delta_{q_1} (+\delta_{\text{complete}}), \\
\mathcal{C}_{q_1} &= 2\delta_{q_1} + \delta_{p_2} + \delta_{r_2} (+\delta_{\text{complete}}), \\
\mathcal{C}_{p_2} &= \delta_{p_2}, \\
\mathcal{C}_{r_2} &= \delta_{r_2}, \\
\mathcal{C}_{q_2} &= \delta_{q_2}.
\end{aligned} \tag{3.74}$$

The intersection matrix of \mathcal{C} 's is the same one as before. The intersection diagrams of δ 's for incomplete / complete cases are shown in Figure 7. The diagram for the incomplete case is an E_6 non-Dynkin diagram, which is similar to the $p_0 \rightarrow q_1$ case. But this time there are two $-\frac{3}{2}$ nodes. The intersection matrix is given by

$$-\delta_I \cdot \delta_J = \begin{pmatrix} \frac{3}{2} & 0 & -1 & -\frac{1}{2} & -1 & 0 \\ 0 & 2 & -1 & 0 & 0 & 0 \\ -1 & -1 & 2 & 0 & 0 & 0 \\ -\frac{1}{2} & 0 & 0 & \frac{3}{2} & 0 & -1 \\ -1 & 0 & 0 & 0 & 2 & 0 \\ 0 & 0 & 0 & -1 & 0 & 2 \end{pmatrix}, \tag{3.75}$$

with the same order $I, J = q_1, p_0, p_2, p_1, r_2, q_2$ as before. Note that the intersection of the two $-\frac{3}{2}$ nodes is $\frac{1}{2}$.

Again, there is only one **32** at $s = 0$ as two-cycles J (3.44) satisfying $J \cdot J = -\frac{3}{2}$. For the complete case, δ_{complete} bridges the two $-\frac{3}{2}$ nodes and forms the ordinary E_7 intersection diagram.

$p_0 \rightarrow p_1 \rightarrow r_2$ case

If r_2 is blown up after p_1 , the relations among \mathcal{C} 's and δ 's are found to be

$$\begin{aligned}
\mathcal{C}_{p_0} &= \delta_{p_0} + \delta_{r_2} (+\delta_{\text{complete}}), \\
\mathcal{C}_{p_1} &= \delta_{p_1}, \\
\mathcal{C}_{r_2} &= 2\delta_{r_2} + \delta_{p_2} + \delta_{q_1} (+\delta_{\text{complete}}), \\
\mathcal{C}_{q_1} &= \delta_{q_1}, \\
\mathcal{C}_{p_2} &= \delta_{p_2}, \\
\mathcal{C}_{q_2} &= \delta_{q_2},
\end{aligned} \tag{3.76}$$

and the intersection diagrams of δ 's are as shown in Figure 8. This time, the diagram for the incomplete case is a D_6 non-Dynkin diagram. There are two nodes with self intersections

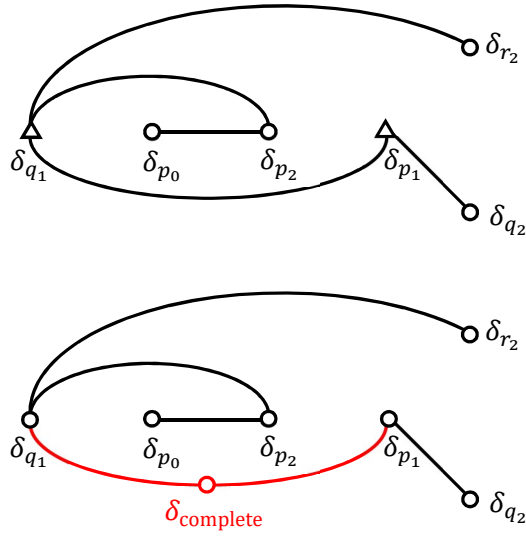


Figure 7. Incomplete/complete intersection diagrams of $SO(12) \rightarrow E_7 : p_1\text{-first} (p_0 \rightarrow p_1 \rightarrow q_1)$ case.

$-\frac{3}{2}$ and their mutual intersection is $\frac{1}{2}$. As before, only one **32** appears at $s = 0$ as $J \cdot J = -\frac{3}{2}$ states. For the complete case, δ_{complete} bridges the two $-\frac{3}{2}$ nodes and forms the ordinary E_7 intersection diagram.

This exhausts all the possibilities of changing the order of the singularities we blow up.

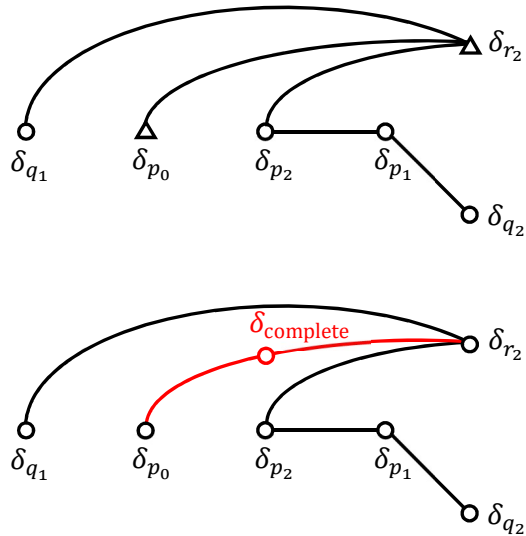


Figure 8. Incomplete/complete intersection diagrams of $SO(12) \rightarrow E_7 : p_1\text{-first} (p_0 \rightarrow p_1 \rightarrow r_2)$ case.

3.6 Comparison with the results of the M-theory Coulomb branch analysis

In the previous sections we have obtained *four* distinct incomplete intersection diagrams of the fibers at the codimension-two singularity. Let us compare our results with those obtained by the M-theory Coulomb branch analysis [14].

In general, F-theory compactifications on Calabi-Yau four-folds are dual to M-theory compactifications on Calabi-Yau four-folds, which present three-dimensional $\mathcal{N} = 2$ supersymmetric gauge theories. The geometry of the Calabi-Yau four-fold determines the structure of the gauge theory. In particular, the codimension-one singularity decides the gauge group, and the network of the resolution corresponds to the structure of the classical Coulomb phase since the resolution corresponds to the symmetry breaking.

We consider three-dimensional gauge theory with a gauge group G and with N_f chiral multiplets in a representation \mathbf{R}_f . We set the masses of the chiral multiplets to zero. In addition, we assume that there is no classical Chern-Simons term. The vector multiplet in the adjoint representation includes a real scalar field ϕ . In general, the gauge group G breaks to $U(1)^r$ by the VEVs of the scalar, where $r = \text{rank}(G)$. We choose the fundamental Weyl chamber as

$$\vec{\alpha}_i \cdot \vec{\phi} > 0, \quad (3.77)$$

where $\vec{\alpha}_i$ ($i = 1, 2, \dots, r$) are the simple roots of G . $\vec{\phi} = (\phi^1, \phi^2, \dots, \phi^r)$ are the VEVs in the Cartan subalgebra of G .

Now we have the chiral multiplets, which make a substructure in the Coulomb branch. The Lagrangian includes the mass terms of the chiral multiplets $Q^{(f)}$:

$$\mathcal{L}_{\text{mass}} = \sum_f \left| \phi Q^{(f)} \right|^2 = \sum_f \left| \vec{\phi} \cdot \vec{\omega}_f \right|^2 \left| Q^{(f)} \right|^2, \quad (3.78)$$

where $\vec{\omega}_f$ are weights of \mathbf{R}_f representation. Note that when $\vec{\phi} \cdot \vec{\omega}_f = 0$, the corresponding matter becomes massless.

We can classify the regions of the Coulomb branch. A region is bounded by the zero loci of $\vec{\phi} \cdot \vec{\omega}_f$, namely, it is characterized by $\vec{\phi} \cdot \vec{\omega}_f > 0$ or $\vec{\phi} \cdot \vec{\omega}_f < 0$. However, not all regions are allowed since we are working on the fundamental Weyl chamber (3.77). The allowed regions of the Coulomb branch are completely classified by the decorated box graphs defined by a collection of boxes with signs (or colors) [14].

Although the analysis of [14] is based on the Coulomb branch of the three-dimensional M-theory, which basically applies to a resolution of a Calabi-Yau four-fold such as [15–18], it is interesting to compare our results with the corresponding box graphs obtained in [14] since the scalars of the five-dimensional M-theory, which are supposed to describe the resolution of a Calabi-Yau three-fold, partly comprise the three-dimensional scalars.

In [14], the intersection diagrams for the singularity enhancement $SO(12) \rightarrow E_7$ are given in Figure 33 of that paper. We can see that the intersection diagrams for incomplete resolutions shown in Figures 5, 7 and 8 of the present paper are the ones at the bottom, the third from the bottom and the second from the top of the left column of Figure 33 of [14]. Also, the (lower) diagram in Figure 2 of this paper is the diagram in the right column of

Figure 33 of [14]. Thus, all the four intersection diagrams we found here have corresponding box graphs obtained in [14] describing different phases of the three-dimensional gauge theory. Note that any two of them are not adjacent to each other in the seven graphs of Figure 33 of [14]. This is consistent, as the two adjacent graphs of [14] are related by a flop, and the change of the order of the singularities is not a flop. Indeed, we do not have any conifold singularities until we consider a complete resolution. This is one of the differences between the resolutions in six and four dimensions.

4 $E_7 \rightarrow E_8$

4.1 Incomplete resolution: Blowing up p_2 first

4.1.1 Blowing up process

In this case we take $f_{n+8} = s$ with setting $g_{n+12} = 1$, $f_8 = g_{12} = 0$ in (2.17) and (2.18) :

$$\begin{aligned} f(z, s) &= sz^3, \\ g(z, s) &= z^5. \end{aligned} \tag{4.1}$$

At $s \neq 0$, the orders of f , g and Δ in z are $(3, 5, 9)$, while at $s = 0$, they satisfy $(\geq 4, 5, 10)$. Hence it describes the enhancement $III^* \rightarrow II^*$ ($E_7 \rightarrow E_8$) of the Kodaira type.

$\Phi(x, y, z, s) = 0$ has a codimension-one singularity at $p_0 = (0, 0, 0, s)$. The concrete process of the incomplete resolution goes as follows (an exceptional curve arising from blowing up a singularity p will be denoted by \mathcal{C}_p):

1st blow up

Chart 1_x

$$\begin{aligned} \Phi(x, xy_1, xz_1, s) &= x^2 \Phi_x(x, y_1, z_1, s), \\ \Phi_x(x, y_1, z_1, s) &= sx^2 z_1^3 + x^3 z_1^5 + x - y_1^2. \\ \mathcal{C}_{p_0} \text{ in } 1_x &: x = 0, \quad y_1 = 0. \\ \text{Singularities} &: \text{None} \end{aligned} \tag{4.2}$$

Chart 1_y \mathcal{C}_{p_0} is not visible in this chart.

Chart 1_z

$$\begin{aligned} \Phi(x_1 z, y_1 z, z, s) &= z^2 \Phi_z(x_1, y_1, z, s), \\ \Phi_z(x_1, y_1, z, s) &= z(x_1 z s + x_1^3 + z^2) - y_1^2. \\ \mathcal{C}_{p_0} \text{ in } 1_z &: z = 0, \quad y_1 = 0. \\ \text{Singularities} &: (x_1, y_1, z, s) = (0, 0, 0, s). \end{aligned} \tag{4.3}$$

We refer to this singularity as p_1 .

2nd blow up

Chart 2_{zx}

$$\begin{aligned}
\Phi_z(x_1, x_1 y_2, x_1 z_2, s) &= x_1^2 \Phi_{zx}(x_1, y_2, z_2, s), \\
\Phi_{zx}(x_1, y_2, z_2, s) &= z_2 x_1 (z_2(s + z_2) + x_1) - y_2^2. \\
\mathcal{C}_{p_1} \text{ in } 2_{zx} &: x_1 = 0, \quad y_2 = 0. \\
\text{Singularities} &: (x_1, y_2, z_2, s) = (0, 0, -s, s)(= q_2), (0, 0, 0, s)(= p_2). \quad (4.4)
\end{aligned}$$

Here we see two singularities on \mathcal{C}_{p_1} which coincide with each other at $s = 0$.

Chart 2_{zy} \mathcal{C}_{p_1} is not visible in this chart.

Chart 2_{zz}

$$\begin{aligned}
\Phi_z(x_2 z, y_2 z, z, s) &= z^2 \Phi_{zz}(x_2, y_2, z, s), \\
\Phi_{zz}(x_2, y_2, z, s) &= z (s x_2 + z x_2^3 + 1) - y_2^2. \\
\mathcal{C}_{p_1} \text{ in } 2_{zz} &: z = 0, \quad y_2 = 0. \\
\text{Singularities} &: (x_2, y_2, z, s) = \left(-\frac{1}{s}, 0, 0, s\right). \quad (4.5)
\end{aligned}$$

This singularity is q_2 , which is also seen in chart 2_{zx} . At this stage, we have two singularities p_2 and q_2 . In this section we blow up p_2 first. We can see this singularity in chart 2_{zx} only, so we consider $\Phi_{zx}(x_1, y_2, z_2, s)$ in the next blow up.

3rd blow up

Chart 3_{zxx}

$$\begin{aligned}
\Phi_{zx}(x_1, x_1 y_3, x_1 z_3, s) &= x_1^2 \Phi_{zxx}(x_1, y_3, z_3, s), \\
\Phi_{zxx}(x_1, y_3, z_3, s) &= z_3 x_1 (s z_3 + z_3^2 x_1 + 1) - y_3^2. \\
\mathcal{C}_{p_2} \text{ in } 3_{zxx} &: x_1 = 0, \quad y_3 = 0. \\
\text{Singularities} &: (x_1, y_3, z_3, s) = \left(0, 0, -\frac{1}{s}, s\right)(= r_3), (0, 0, 0, s)(= p_3). \quad (4.6)
\end{aligned}$$

We name the first singularity r_3 , and the second singularity p_3 .

Chart 3_{zxy} Regular.

Chart 3_{zxz}

$$\begin{aligned}
\Phi_{zx}(x_3 z_2, y_3 z_2, z_2, s) &= z_2^2 \Phi_{zxz}(x_3, y_3, z_2, s), \\
\Phi_{zxz}(x_3, y_3, z_2, s) &= z_2 x_3 (s + z_2 + x_3) - y_3^2. \\
\mathcal{C}_{p_2} \text{ in } 3_{zxz} &: z_2 = 0, \quad y_3 = 0. \\
\text{Singularities} &: (x_3, y_3, z_2, s) = (0, 0, -s, s)(= q_2), (0, 0, 0, s)(= q_3), \\
&\quad (-s, 0, 0, s)(= r_3). \quad (4.7)
\end{aligned}$$

The first singularity is not on \mathcal{C}_{p_2} unless $s = 0$; this is q_2 . We name the second singularity q_3 . The third one is r_3 already seen in chart 3_{zxx} .

When $s \rightarrow 0$, the three singularities q_2 , q_3 and r_3 in chart 3_{zxx} coincide with each other, and which one we blow up next affects the proceeding process. In this section, we consider the case q_3 is blown up next. On the other hand, p_3 in chart 3_{zxx} is separated from these points even when $s \rightarrow 0$ and can be blown up independently. We leave the blow-up of p_3 until later and work on the blow-up of q_3 .

4th blow up at q_3 We next blow up q_3 . Using $\Phi_{zxz}(x_3, y_3, z_2, s)$, we find

Chart 4_{zxzx}

$$\begin{aligned}\Phi_{zxz}(x_3, x_3 y_4, x_3 z_4, s) &= x_3^2 \Phi_{zxzx}(x_3, y_4, z_4, s), \\ \Phi_{zxzx}(x_3, y_4, z_4, s) &= z_4 (s + z_4 x_3 + x_3) - y_4^2. \\ \mathcal{C}_{q_3} \text{ in } 4_{zxzx} &: x_3 = 0, \quad y_4^2 = s z_4. \\ \text{Singularities} &: (x_3, y_4, z_4, s) = (-s, 0, 0, s).\end{aligned}\tag{4.8}$$

This is r_3 , which is not on \mathcal{C}_{q_3} unless $s = 0$.

Chart 4_{zxzy} Regular.

Chart 4_{zxzz}

$$\begin{aligned}\Phi_{zxz}(x_4 z_2, y_4 z_2, z_2, s) &= z_2^2 \Phi_{zxzz}(x_4, y_4, z_2, s), \\ \Phi_{zxzz}(x_4, y_4, z_2, s) &= s x_4 + z_2 x_4 (x_4 + 1) - y_4^2. \\ \mathcal{C}_{q_3} \text{ in } 4_{zxzz} &: z_2 = 0, \quad y_4^2 = s x_4. \\ \text{Singularities} &: (x_4, y_4, z_2, s) = (0, 0, -s, s).\end{aligned}\tag{4.9}$$

This is q_2 , which is not on \mathcal{C}_{q_3} unless $s = 0$, either. r_3 and q_2 coincide with each other at $s = 0$ before blowing up q_3 ; but after the blow up, they are never the same point even when $s = 0$. Thus we can blow them up independently.

5th blow up at r_3 To blow up r_3 in chart 4_{zxzx} (4.8), we shift the x_3 coordinate so that this singularity is represented as $(0, 0, 0, s)$ in the new coordinate \tilde{x}_3 :

$$\Psi_{zxzx}(\tilde{x}_3, y_4, z_4, s) \equiv \Phi_{zxzx}(\tilde{x}_3 - s, y_4, z_4, s).\tag{4.10}$$

Then it can be verified that no singularity arises in charts 5_{zxzx*} below. The exceptional curves are:

Chart 5_{zxzxx}

$$\begin{aligned}\Psi_{zxzx}(\tilde{x}_3, \tilde{x}_3 y_5, \tilde{x}_3 z_5, s) &= \tilde{x}_3^2 \Psi_{zxzxx}(\tilde{x}_3, y_5, z_5, s), \\ \Psi_{zxzxx}(\tilde{x}_3, y_5, z_5, s) &= z_5^2 (\tilde{x}_3 - s) + z_5 - y_5^2. \\ \mathcal{C}_{r_3} \text{ in } 5_{zxzxx} &: \tilde{x}_3 = 0, \quad y_5^2 = -s z_5^2 + z_5.\end{aligned}\tag{4.11}$$

Chart 5_{zxzxy} Invisible.

Chart 5_{zxzxz}

$$\begin{aligned}\Psi_{zxzx}(x_5 z_4, y_5 z_4, z_4, s) &= z_4^2 \Psi_{zxzx}(x_5, y_5, z_4, s), \\ \Psi_{zxzx}(x_5, y_5, z_4, s) &= -s + z_4 x_5 + x_5 - y_5^2. \\ \mathcal{C}_{r_3} \text{ in } 5_{zxzxz} &: z_4 = 0, \quad y_5^2 = x_5 - s.\end{aligned}\tag{4.12}$$

5th blow up at q_2 Having resolved the singularity r_3 , we turn to the resolution of q_2 in chart 4_{zxzz} (4.9). For this we need a different coordinate shift:

$$\Psi_{zxzz}(x_4, y_4, \tilde{z}_2, s) \equiv \Phi_{zxzz}(x_4, y_4, \tilde{z}_2 - s, s).\tag{4.13}$$

Then Ψ_{zxzz} has a singularity at $(x_4, y_4, \tilde{z}_2, s) = (0, 0, 0, s)$. Again, charts 5_{zxzz*} below have no singularity. The exceptional curves are:

Chart 5_{zxzzx}

$$\begin{aligned}\Psi_{zxzz}(x_4, x_4 y_5, x_4 z_5, s) &= x_4^2 \Psi_{zxzz}(x_4, y_5, z_5, s), \\ \Psi_{zxzz}(x_4, y_5, z_5, s) &= -s + z_5 x_4 + z_5 - y_5^2. \\ \mathcal{C}_{q_2} \text{ in } 5_{zxzzx} &: x_4 = 0, \quad y_5^2 = z_5 - s.\end{aligned}\tag{4.14}$$

Chart 5_{zxzzy} We omit the details.

Chart 5_{zxzzz}

$$\begin{aligned}\Psi_{zxzz}(x_5 \tilde{z}_2, y_5 \tilde{z}_2, \tilde{z}_2, s) &= \tilde{z}_2^2 \Psi_{zxzz}(x_5, y_5, \tilde{z}_2, s), \\ \Psi_{zxzz}(x_5, y_5, \tilde{z}_2, s) &= x_5^2 (-s + \tilde{z}_2) + x_5 - y_5^2. \\ \mathcal{C}_{q_2} \text{ in } 5_{zxzzz} &: \tilde{z}_2 = 0, \quad y_5^2 = -s x_5^2 + x_5.\end{aligned}\tag{4.15}$$

4th blow up at p_3 Let us return to chart 3_{zxzx} and blow up the remaining p_3 (4.6).

Chart 4_{zxzx}

$$\begin{aligned}\Phi_{zxzx}(x_1, x_1 y_4, x_1 z_4, s) &= x_1^2 \Phi_{zxzx}(x_1, y_4, z_4, s), \\ \Phi_{zxzx}(x_1, y_4, z_4, s) &= s z_4^2 x_1 + z_4^3 x_1^3 + z_4 - y_4^2. \\ \mathcal{C}_{p_3} \text{ in } 4_{zxzx} &: x_1 = 0, \quad y_4^2 = z_4. \\ \text{Singularities} &: \text{None.}\end{aligned}\tag{4.16}$$

Chart 4_{zxxy} Regular .

Chart 4_{zxzxz}

$$\begin{aligned}\Phi_{zxzx}(x_4 z_3, y_4 z_3, z_3, s) &= z_3^2 \Phi_{zxzx}(x_4, y_4, z_3, s), \\ \Phi_{zxzx}(x_4, y_4, z_3, s) &= s z_3 x_4 + z_3^3 x_4^2 + x_4 - y_4^2. \\ \mathcal{C}_{p_3} \text{ in } 4_{zxzxz} &: z_3 = 0, \quad y_4^2 = x_4. \\ \text{Singularities} &: (x_4, y_4, z_3, s) = (0, 0, -\frac{1}{s}, s).\end{aligned}\tag{4.17}$$

This singularity is not on \mathcal{C}_{p_3} even when $s = 0$; this is r_3 (see (4.6)) and is blown up as in (4.11) and (4.12).

The whole process of the incomplete resolution of the codimension-two singularity enhancement from E_7 to E_8 is summarized in Table 5.

Table 5. $E_7 \rightarrow E_8$: Incomplete case when p_2 is blown up first ($p_0 \rightarrow p_1 \rightarrow p_2 \rightarrow q_3$).

	1st blow up	2nd blow up	3rd blow up	4th blow up	5th blow up
$\mathcal{Q}_0 \rightarrow$	$\mathcal{Q}_1(0:0:1) \rightarrow$	$\mathcal{Q}_2(1:0:0) \rightarrow$ $q_2(1:0:-s)$	$\mathcal{Q}_3(1:0:0) \rightarrow$ $\mathcal{Q}_3(0:0:1) \rightarrow$ $q_2(0:0:1)(z_2 = -s)$ $r_3(-s:0:1)$	regular regular $\mathcal{Q}_2(0:0:1)(z_2 = -s) \rightarrow$ $\mathcal{Q}_3(1:0:0)(x_3 = -s) \rightarrow$	regular regular

4.1.2 Intersection diagram at $s = 0$

Exceptional curves δ_I at $s = 0$ are defined from \mathcal{C}_I ($I \in \{p_0, p_1, p_2, q_3, r_3, q_2, p_3\}$). One can see from the explicit blowing up process that the intersection patterns of \mathcal{C} 's and δ 's are E_7 and A_7 , respectively (see Figure 9 below). As explained in section 3.1.3, the $s \rightarrow 0$ limit of \mathcal{C}_I is derived through the careful lift-ups of \mathcal{C}_I and δ_I from the chart where they are originally defined to the charts arise via the subsequent blow-ups. In this case, we have

$$\begin{aligned}
\mathcal{C}_{p_0} &= \delta_{p_0}, \\
\mathcal{C}_{p_1} &= \delta_{p_1}, \\
\mathcal{C}_{p_2} &= \delta_{p_2}, \\
\mathcal{C}_{q_3} &= 2\delta_{q_3} + \delta_{r_3} + \delta_{q_2}, \\
\mathcal{C}_{r_3} &= \delta_{r_3}, \\
\mathcal{C}_{q_2} &= \delta_{q_2}, \\
\mathcal{C}_{p_3} &= \delta_{p_3}.
\end{aligned} \tag{4.18}$$

The intersection matrix of \mathcal{C} 's is the minus of the ordinary E_7 Cartan matrix

$$-\mathcal{C}_I \cdot \mathcal{C}_J = \begin{pmatrix} 2 & -1 & 0 & 0 & 0 & 0 & 0 \\ -1 & 2 & -1 & 0 & 0 & 0 & 0 \\ 0 & -1 & 2 & -1 & 0 & 0 & -1 \\ 0 & 0 & -1 & 2 & -1 & 0 & 0 \\ 0 & 0 & 0 & -1 & 2 & -1 & 0 \\ 0 & 0 & 0 & 0 & -1 & 2 & 0 \\ 0 & 0 & -1 & 0 & 0 & 0 & 2 \end{pmatrix}, \tag{4.19}$$

where $I, J = p_0, p_3, p_2, q_3, p_1, q_2, r_3$ in this order. Then the relations (4.18) imply that the intersection matrix of δ 's is

$$-\delta_I \cdot \delta_J = \begin{pmatrix} 2 & -1 & 0 & 0 & 0 & 0 & 0 \\ -1 & 2 & -1 & 0 & 0 & 0 & 0 \\ 0 & -1 & 2 & 0 & 0 & 0 & -1 \\ 0 & 0 & 0 & \frac{3}{2} & 0 & -1 & -1 \\ 0 & 0 & 0 & 0 & 2 & -1 & 0 \\ 0 & 0 & 0 & -1 & -1 & 2 & 0 \\ 0 & 0 & -1 & -1 & 0 & 0 & 2 \end{pmatrix}. \tag{4.20}$$

This is the minus of the A_7 Cartan matrix except that one of the δ 's ($= \delta_{q_3}$) has self-intersection $-\frac{3}{2}$, which equals to the minus of the length squared of a weight in the **56** representation of E_7 . The result is shown in Figure 9. For the two-cycles at $s = 0$

$$J \equiv \sum_{I=p_0, p_3, p_2, q_3, p_1, q_2, r_3} n_I \delta_I \quad (n_I \in \mathbb{Z}), \quad (4.21)$$

one can show by using (4.20) that

$$\begin{aligned} \#(J \cdot J = -2) &= 126, \\ \#(J \cdot J = -\frac{3}{2}) &= 56. \end{aligned} \quad (4.22)$$

They respectively are the adjoint (without Cartan part) and **56** representations of E_7 . The latter consists of 28 elements with $n_I \geq 0$ for all I and 28 elements with $n_I \leq 0$ for all I . Again, there is only a single **56** representation, indicating that it is a half-hypermultiplet.

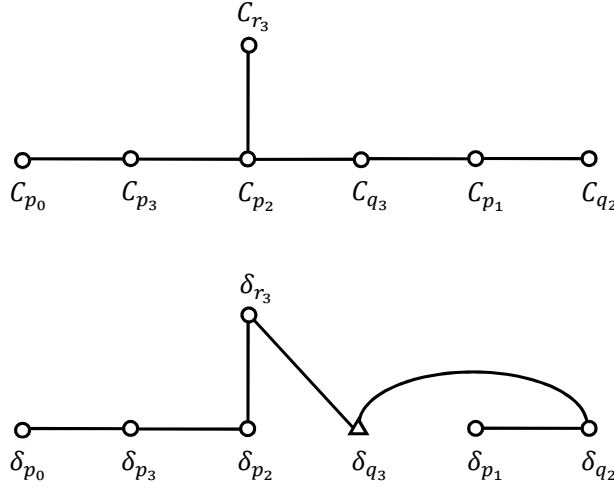


Figure 9. Generic E_7 intersection diagram at $s \neq 0$ (upper) and incomplete intersection diagram at $s = 0$ (lower) of $E_7 \rightarrow E_8 : p_2$ -first ($p_0 \rightarrow p_1 \rightarrow p_2 \rightarrow q_3$) case.

4.2 Complete resolution

We will now consider the complete resolution. This can be achieved by taking $f_{n+8} = s^2$ instead of s . This amounts to replacing s in (4.1) with s^2 . Similarly to the previous sections, we find an additional isolated codimension-two conifold singularity after we blow up q_3 . As shown in red in Table 6, this new singularity, which we denote by r_4 , arises at $(1 : 0 : -1)$ on the \mathbb{P}^2 particularly at $s = 0$. This adds an extra node to the incomplete intersection diagram to form the correct E_8 Dynkin diagram as we show in Figure 10. To see how the intersection matrix is modified, we repeat the argument given in section 3.2.2. By carefully lifting up \mathcal{C} 's and δ 's into the local coordinate system of the small resolution, we find the

modified relations

$$\begin{aligned}
\mathcal{C}_{p_0} &= \delta_{p_0}, \\
\mathcal{C}_{p_1} &= \delta_{p_1}, \\
\mathcal{C}_{p_2} &= \delta_{p_2}, \\
\mathcal{C}_{q_3} &= 2\delta_{q_3} + \delta_{r_3} + \delta_{q_2} + \delta_{\text{complete}}, \\
\mathcal{C}_{r_3} &= \delta_{r_3}, \\
\mathcal{C}_{q_2} &= \delta_{q_2}, \\
\mathcal{C}_{p_3} &= \delta_{p_3}.
\end{aligned} \tag{4.23}$$

One can then verify that: if the intersection matrix of these eight δ 's is the minus of the ordinary E_8 Cartan matrix, the intersection matrix of \mathcal{C} 's (4.19) is reproduced. Therefore, the node δ_{q_3} , which was formerly represented by a triangle in Figure 9, is now an ordinary node consisting of the root system of E_8 as in Figure 10.

Table 6. $E_7 \rightarrow E_8$: Complete case when p_2 is blown up first ($p_0 \rightarrow p_1 \rightarrow p_2 \rightarrow q_3$).

	1st blow up	2nd blow up	3rd blow up	4th blow up	5th blow up
$\widehat{\mathcal{P}}_0 \rightarrow$	$\widehat{\mathcal{P}}_1(0 : 0 : 1) \rightarrow$	$\widehat{\mathcal{P}}_2(1 : 0 : 0) \rightarrow$ $q_2(1 : 0 : -s^2)$	$\widehat{\mathcal{P}}_3(1 : 0 : 0) \rightarrow$ $\widehat{\mathcal{Q}}_3(0 : 0 : 1) \rightarrow$ $q_2(0 : 0 : 1)(z_2 = -s^2)$ $r_3(-s^2 : 0 : 1)$	regular $\widehat{\mathcal{R}}_4(1 : 0 : -1; s = 0)(\text{codim.2}) \rightarrow$ $\widehat{\mathcal{Q}}_2(0 : 0 : 1)(z_2 = -s^2) \rightarrow$ $\widehat{\mathcal{R}}_3(1 : 0 : 0)(x_3 = -s^2) \rightarrow$	regular regular regular

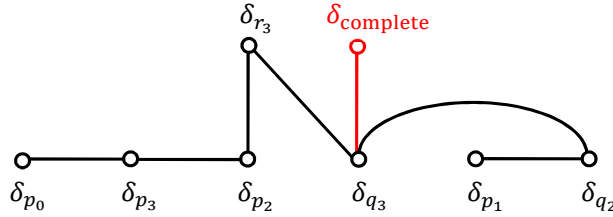


Figure 10. Complete E_8 intersection diagram of $E_7 \rightarrow E_8$: p_2 -first ($p_0 \rightarrow p_1 \rightarrow p_2 \rightarrow q_3$) case.

4.3 Incomplete/complete resolutions: Blowing up q_2 first

As we did for $SO(12) \rightarrow E_7$, we can change the order of the blow-ups to obtain a different intersection diagram. For instance, we can choose q_2 instead of p_2 for the 3rd blow up. The

procedures are analogous to the previous cases so we report only the results.

For the incomplete resolution, the whole process of the blow-ups is as shown in Table 7. We use the same notation for \mathcal{C} 's (and hence for δ 's) as was used in the p_2 -first case. Then the intersection pattern of \mathcal{C} 's for the q_2 -first case is the same E_7 Dynkin diagram with the p_2 -first case given in Figure 9 and their intersection matrix is also the same with (4.19). The intersection pattern of δ 's, however, is different from the one (A_7) given in Figure 9. This time, it is E_7 (see Figure 11 below).

One can verify the relations

$$\begin{aligned}
\mathcal{C}_{p_0} &= \delta_{p_0} + \delta_{q_2}, \\
\mathcal{C}_{p_1} &= \delta_{p_1}, \\
\mathcal{C}_{q_2} &= 2\delta_{q_2} + 2\delta_{p_2} + 2\delta_{p_3} + \delta_{q_3} + \delta_{r_3}, \\
\mathcal{C}_{p_2} &= \delta_{p_2}, \\
\mathcal{C}_{p_3} &= \delta_{p_3}, \\
\mathcal{C}_{q_3} &= \delta_{q_3}, \\
\mathcal{C}_{r_3} &= \delta_{r_3}.
\end{aligned} \tag{4.24}$$

Then the intersection matrix among δ 's has two $-\frac{3}{2}$ nodes as shown in Figure 11. The intersection among these two nodes is $\frac{1}{2}$. As is the same as the previous examples, one can form $28 + 28$ different linear combinations of δ 's with non-negative and non-positive integer coefficients such that they have self-intersection $-\frac{3}{2}$, giving a single **56** representation.

Table 7. $E_7 \rightarrow E_8$: Incomplete case when q_2 is blown up first ($p_0 \rightarrow p_1 \rightarrow q_2$).

	1st blow up	2nd blow up	3rd blow up	4th blow up	5th blow up
$\mathcal{P}_0 \rightarrow$	$\mathcal{P}_1(0 : 0 : 1) \rightarrow$	$\mathcal{P}_2(1 : 0 : -s) \rightarrow$ $p_2(1 : 0 : 0)$	regular $\mathcal{P}_2(0 : 0 : 1)(\tilde{z}_2 = s) \rightarrow$	$\mathcal{P}_3(1 : 0 : 0) \rightarrow$ $\mathcal{Q}_3(0 : 0 : 1) \rightarrow$ $\mathcal{R}_3(1 : 0 : -1) \rightarrow$	regular regular regular

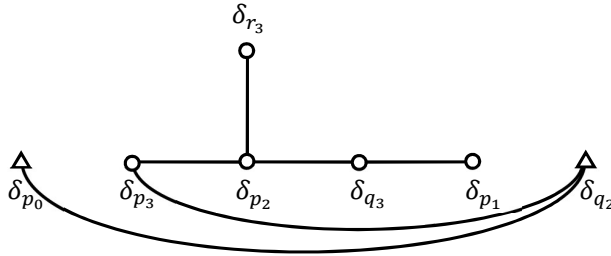


Figure 11. Incomplete intersection diagram of $E_7 \rightarrow E_8$: q_2 -first ($p_0 \rightarrow p_1 \rightarrow q_2$) case.

In the complete case, the 3rd blow up at q_2 does not end with a smooth configuration but an isolated codimension-two conifold singularity remains at the intersection of δ_{p_0} and δ_{q_2} at $s = 0$ (see Table 8). By a small resolution of this, the relations are modified as

$$\begin{aligned}
\mathcal{C}_{p_0} &= \delta_{p_0} + \delta_{q_2} + \delta_{\text{complete}}, \\
\mathcal{C}_{p_1} &= \delta_{p_1}, \\
\mathcal{C}_{q_2} &= 2\delta_{q_2} + 2\delta_{p_2} + 2\delta_{p_3} + \delta_{q_3} + \delta_{r_3} + \delta_{\text{complete}}, \\
\mathcal{C}_{p_2} &= \delta_{p_2}, \\
\mathcal{C}_{p_3} &= \delta_{p_3}, \\
\mathcal{C}_{q_3} &= \delta_{q_3}, \\
\mathcal{C}_{r_3} &= \delta_{r_3}.
\end{aligned} \tag{4.25}$$

Demanding that the intersection matrix among δ 's is the minus of the proper E_8 Cartan matrix is consistent with the intersection matrix among \mathcal{C} 's. As a result, we obtain Figure 12.

Table 8. $E_7 \rightarrow E_8$: Complete case when q_2 is blown up first ($p_0 \rightarrow p_1 \rightarrow q_2$).

	1st blow up	2nd blow up	3rd blow up	4th blow up	5th blow up
$\mathcal{P}_0 \rightarrow$	$\mathcal{P}_1(0 : 0 : 1) \rightarrow$	$\mathcal{P}_2(1 : 0 : -s) \rightarrow$ $p_2(1 : 0 : 0)$	$\mathcal{P}_3(1 : 0 : 0; s = 0)(\text{codim.2}) \rightarrow$ $\mathcal{P}_2(0 : 0 : 1)(\tilde{z}_2 = s) \rightarrow$	regular $\mathcal{P}_3(1 : 0 : 0) \rightarrow$	regular
				$\mathcal{Q}_3(0 : 0 : 1) \rightarrow$	regular
				$\mathcal{R}_3(1 : 0 : -1) \rightarrow$	regular

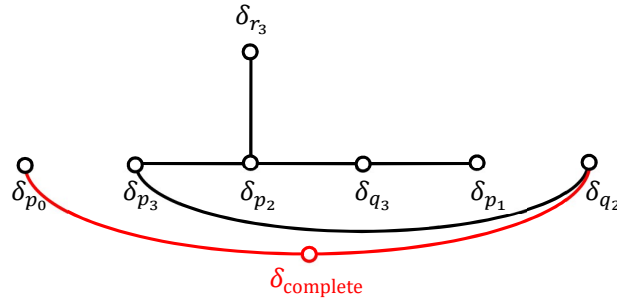


Figure 12. Complete E_8 intersection diagram of $E_7 \rightarrow E_8$: q_2 -first ($p_0 \rightarrow p_1 \rightarrow q_2$) case.

4.4 Other inequivalent orderings

Let us summarize what other types of intersection diagrams are obtained for the enhancement $E_7 \rightarrow E_8$ if we choose other orderings of the blow-ups. So far, we have derived the intersection diagrams for blow-ups with orders $p_0 \rightarrow p_1 \rightarrow p_2 \rightarrow q_3$ and $p_0 \rightarrow p_1 \rightarrow q_2$. As we can see in the column “3rd blow up” in Table 5, after blowing up p_2 , the three singular points q_3 , q_2 and r_3 become an identical point $(0 : 0 : 1)$ on the \mathbb{P}^2 at $s = 0$ (see also (4.7)). Therefore, besides the case when q_3 is blown up after p_2 as discussed in sections 4.1 and 4.2⁶, there are two other options: We can blow up either q_2 or r_3 after the blow up of p_2 .

$p_0 \rightarrow p_1 \rightarrow p_2 \rightarrow q_2$ case

If we blow up q_2 after p_2 , the relations between \mathcal{C} 's and δ 's are given by

$$\begin{aligned}
\mathcal{C}_{p_0} &= \delta_{p_0}, \\
\mathcal{C}_{p_1} &= \delta_{p_1}, \\
\mathcal{C}_{p_2} &= \delta_{p_2} + \delta_{q_2} (+\delta_{\text{complete}}), \\
\mathcal{C}_{q_2} &= 2\delta_{q_2} + \delta_{q_3} + \delta_{r_3} (+\delta_{\text{complete}}), \\
\mathcal{C}_{q_3} &= \delta_{q_3}, \\
\mathcal{C}_{r_3} &= \delta_{r_3}, \\
\mathcal{C}_{p_3} &= \delta_{p_3}.
\end{aligned} \tag{4.26}$$

The intersection diagram of \mathcal{C} 's is the E_7 Dynkin diagram as before. The intersection diagrams of δ 's for incomplete / complete cases are shown in Figure 13. For the incomplete case, it is an E_7 non-Dynkin diagram with two $-\frac{3}{2}$ nodes (the intersection among them is $\frac{1}{2}$), while for the complete case, it is proper E_8 Dynkin diagram. Again, there is only one **56** at $s = 0$ as two-cycles J (3.44) with $J \cdot J = -\frac{3}{2}$.

$p_0 \rightarrow p_1 \rightarrow p_2 \rightarrow r_3$ case

If we blow up r_3 after p_2 , the relations between \mathcal{C} 's and δ 's are given by

$$\begin{aligned}
\mathcal{C}_{p_0} &= \delta_{p_0}, \\
\mathcal{C}_{p_1} &= \delta_{p_1} + \delta_{r_3} (+\delta_{\text{complete}}), \\
\mathcal{C}_{p_2} &= \delta_{p_2}, \\
\mathcal{C}_{r_3} &= 2\delta_{r_3} + \delta_{q_2} + \delta_{q_3} (+\delta_{\text{complete}}), \\
\mathcal{C}_{q_2} &= \delta_{q_2}, \\
\mathcal{C}_{q_3} &= \delta_{q_3}, \\
\mathcal{C}_{p_3} &= \delta_{p_3}.
\end{aligned} \tag{4.27}$$

The intersection diagrams are shown in Figure 14. The diagram for the incomplete case is a D_7 non-Dynkin diagram with two $-\frac{3}{2}$ nodes (their intersection is $\frac{1}{2}$). Again, there is only one **56** at $s = 0$.

⁶ p_3 is always a different point from the three and hence can be blown up independently at any stage.

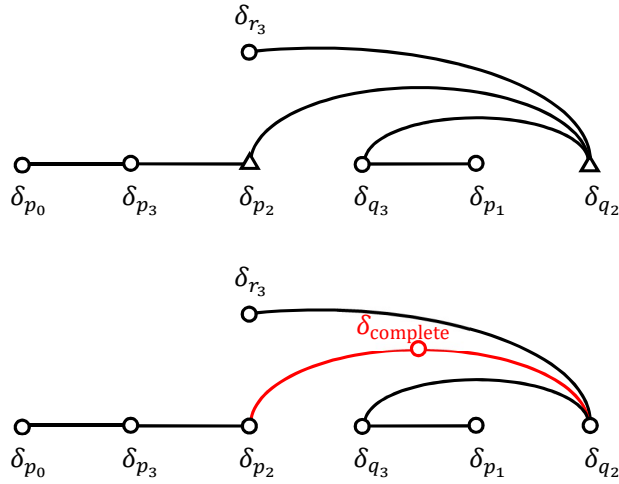


Figure 13. Incomplete/complete intersection diagrams of $E_7 \rightarrow E_8 : p_2$ -first ($p_0 \rightarrow p_1 \rightarrow p_2 \rightarrow q_2$) case.

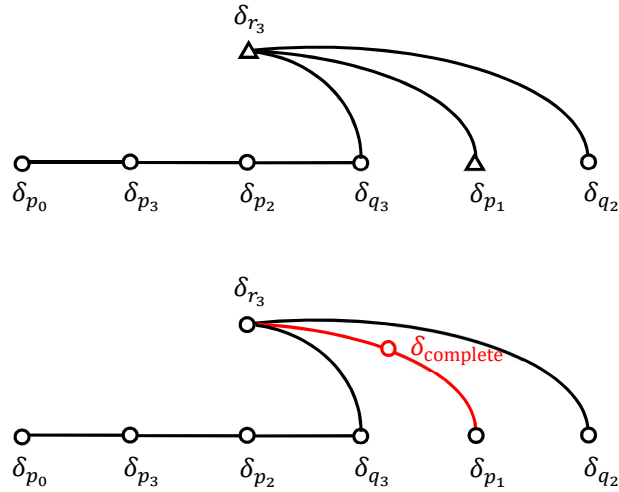


Figure 14. Incomplete/complete intersection diagrams of $E_7 \rightarrow E_8 : p_2$ -first ($p_0 \rightarrow p_1 \rightarrow p_2 \rightarrow r_3$) case.

This exhausts all the possibilities of changing the order of the singularities we blow up. We obtained four sets of incomplete / complete intersection diagrams. Again, each of them corresponds to a box graph on every other row of Figure 44 in [14]. For the p_2 -first cases, Figure 9 (with Figure 10) is equivalent to the one in the right column: Figure 13 and Figure 14 respectively are the fourth and sixth ones from the bottom in the left column. For the q_2 -first case, Figure 11 (with Figure 12) is the second one from the bottom in the left column.

5 Conclusions

We have investigated the resolutions of codimension-two enhanced singularities from $SO(12)$ to E_7 and from E_7 to E_8 in six-dimensional F-theory, where a half-hypermultiplet locally arises for generic complex structures achieving them. A half-hypermultiplet only occurs associated with a Lie algebra allowing a pseudo-real representation, and the above are the two of the three cases in the list of six-dimensional F-theory compactifications [7] that exhibit half-hypermultiplets in the massless matter spectrum. As was already observed in the enhancement from $SU(6)$ to E_6 in [11], we have confirmed that the resolution process does not generically yield as many number of exceptional curves as naively expected from the Kodaira classification of the codimension-one singularities. In the present paper, we have observed similar features such as non-Dynkin intersection diagrams and half-integral intersection numbers of exceptional fibers. Then we have found that the exceptional fibers at the enhanced point form extremal rays of the cone of the positive weights of the relevant pseudo-real representation, explaining why a half-hyper multiplet arises there.

We have also found that a variety of different intersection diagrams of exceptional curves are obtained by altering the ordering of the singularities blown up in the process. They correspond to different “phases” of the three-dimensional M-theory. We have obtained, for both $SO(12) \rightarrow E_7$ and $E_7 \rightarrow E_8$, the intersection diagram on *every other row* of the figures in [14], but not all of them. The phases corresponding to the diagrams we obtained are not the ones related by a flop.

We have presented detailed derivations of the intersection diagrams of the exceptional fibers at the singularity enhanced points. In particular, we have described how an exceptional curve is lifted up on the chart arising due to the subsequent blowing-up process. By carefully examining whether an exceptional curve contains another arising afterwards as a part, we have obtained the intersection matrices as above.

In the complete resolutions, where the colliding brane approaches the stack of branes as $O(s^2)$, we have obtained the full Dynkin diagrams of the group G as the intersection diagram of the fibers at the enhanced point. The extra codimension-two singularity is always a conifold singularity, as was found in the previous example [11].

Although we have studied in this paper the explicit resolutions of the singularities in six dimensions, the technologies we have developed here can also be used in more general settings such as codimension-three singularities in Calabi-Yau four-folds, with or without sections. (In the latter, one may consider the Jacobian fibrations. See e.g. [27].)

It would also be interesting to perform a similar analysis for a singularity with higher rank enhancement. In particular, it has been expected [10] that a codimension-three singularity enhancement from $SU(5)$ to E_7 could yield, without monodromies and with appropriate G -fluxes, the three-generation spectrum of the $E_7/(SU(5) \times U(1)^3)$ supersymmetric coset model [28]. Such a codimension-two singularity enhancement in six dimensions was already studied in [29]. The codimension-three case with a \mathbb{Z}_2 or a larger monodromy was considered in e.g. [30], but was concluded to be not very useful for their purposes. The box graph analysis of [14], on the other hand, predicts the existence of the phases without monodromies, which will serve as basis for models of family unification in F-theory. We

hope to come back to this issue elsewhere.

Finally, massless matter generation in F-theory may also be explained by string junctions stretched between various (p, q) 7-branes near the intersections. Very recently, a new pictorial method to keep track of non-localness of F-theory 7-branes has been developed by drawing a “dessin” on the base of the elliptic fibration [31, 32], which may help understanding how the difference of the resolutions is affected by the geometry near the enhanced point.

Acknowledgments

We thank H. Hayashi, Y. Kimura, H. Otsuka and S. Schafer-Nameki for valuable discussions.

A Symplectic Majorana-Weyl spinors, pseudo-real representations and half-hypermultiplets

A.1 Symplectic Majorana-Weyl spinors

In six(=5+1) dimensions, consider the Dirac equation

$$(i\gamma^\mu \partial_\mu - m)\psi = 0. \quad (\text{A.1})$$

The complex conjugate equation

$$(-i\gamma^{\mu*} \partial_\mu - m)\psi^* = 0 \quad (\text{A.2})$$

can be written in terms of the charge conjugation ψ^c defined by

$$\psi^c \equiv B\psi^* \quad (\text{A.3})$$

with

$$B\gamma^{\mu*} B^{-1} = -\gamma^\mu \quad (\text{A.4})$$

as

$$(i\gamma^\mu \partial_\mu - m)\psi^c = 0. \quad (\text{A.5})$$

This is the same Dirac equation as that ψ obeys. If one could impose the constraint $\psi^c = \psi$ on ψ , one could define a Majorana spinor, but in six dimensions one can not as, if one could do so,

$$\psi = \psi^c = B\psi^* = B(B\psi^*)^* = BB^*\psi, \quad (\text{A.6})$$

but

$$BB^* = -1 \quad (\text{A.7})$$

in six dimensions. Alternatively, one can impose on two Weyl spinors ψ_1, ψ_2 the constraint

$$\psi_1^c = +\psi_2, \quad \psi_2^c = -\psi_1. \quad (\text{A.8})$$

They are called symplectic Majorana-Weyl spinors. Note that in six(=5+1)-dimensions the charge conjugation operation does not flip the chirality so that one can define symplectic Majorana-*Weyl* spinors.

A.2 Pseudo-real representation and symplectic Majorana condition

Let us examine whether one can consistently impose this constraint on a representation space of a Lie group. Let G be a compact Lie group and ρ be its representation on a complex $2n$ -dimensional vector space V :

$$\rho : G \rightarrow GL_{\mathbb{C}}(V) \quad \text{homomorphism.} \quad (\text{A.9})$$

We say ρ is a pseudo-real representation if there exists $P \in GL_{\mathbb{C}}(V)$ such that

$$P(\rho(g))^* P^{-1} = \rho(g) \quad (\text{A.10})$$

for any $g \in G$. $*$ denotes the complex conjugation.

If

$$v' = \rho(g)v, \quad (\text{A.11})$$

then

$$\begin{aligned} P v'^* &= (P(\rho(g))^* P^{-1}) P v^* \\ &= \rho(g) P v^*. \end{aligned} \quad (\text{A.12})$$

Therefore $P v^*$ also transforms as $\mathbf{2n}$.

If $\rho(g)$ can be embedded in $Sp(2n)$, we have

$$\begin{aligned} \rho(g)^T \Omega_{2n} \rho(g) &= \Omega_{2n}, \\ \Omega_{2n} &= \begin{pmatrix} 0 & -1_n \\ 1_n & 0 \end{pmatrix}. \end{aligned} \quad (\text{A.13})$$

Moreover, if ρ is a unitary representation: $\rho(g)^{-1} = \rho(g)^\dagger$, we find

$$\rho(g) = \Omega_{2n} \rho(g)^* \Omega_{2n}^{-1}. \quad (\text{A.14})$$

Thus we can take

$$P = \Omega_{2n}. \quad (\text{A.15})$$

Let us construct such a vector v by using symplectic Majorana(-Weyl) spinors. Let ψ_1, ψ_2 be a pair of n -component column vectors consisting of n symplectic Majorana(-Weyl) spinors, and v be a stack of them. Then

$$\begin{aligned} v &= \begin{pmatrix} \psi_1 \\ \psi_2 \end{pmatrix} \\ &= \begin{pmatrix} -\psi_2^c \\ \psi_1^c \end{pmatrix} \\ &= \begin{pmatrix} 0 & -1_n \\ 1_n & 0 \end{pmatrix} \begin{pmatrix} \psi_1^c \\ \psi_2^c \end{pmatrix} \\ &= \Omega_{2n} \begin{pmatrix} B\psi_1^* \\ B\psi_2^* \end{pmatrix} \\ &= \Omega_{2n}(B \cdot 1_{2n})v^*. \end{aligned} \quad (\text{A.16})$$

In general, this is not consistent as v transforms as a $\mathbf{2n}$ representation whereas v^* as a $\overline{\mathbf{2n}}$ representation. However, for a pseudo-real representation (A.14), we obtain

$$\begin{aligned}\rho(g)v &= \Omega_{2n}\rho(g)^*\Omega_{2n}^{-1}\cdot\Omega_{2n}(B\cdot 1_{2n})v^* \\ &= \Omega_{2n}(B\cdot 1_{2n})\rho(g)^*v^*,\end{aligned}\tag{A.17}$$

which agrees with (A.16). Therefore, for a pseudo-real representation a $2n$ -dimensional representation space can be constructed from n pairs of symplectic Majorana-Weyl spinors.

A.3 $\frac{2n}{2}$ hypermultiplets vs. $\mathbf{2n}$ $\frac{1}{2}$ hypermultiplets

In the previous section we have seen that among $2n$ Weyl fermions in hypermultiplets transforming as a pseudo-real $\mathbf{2n}$ representation one half ($= n$) of them can be expressed as the complex conjugates of the other half ($= n$). In this section we will show that this can be viewed as a restriction of the degrees of freedom of $2n$ (Weyl fermions of) hypermultiplets to $2n$ (“half-Weyl” fermions of) half-hypermultiplets.

We take

$$\begin{aligned}\Gamma^0 &= \sigma_3 \otimes \sigma_3 \otimes i\sigma_2, \\ \Gamma^1 &= \sigma_3 \otimes \sigma_3 \otimes \sigma_1, \\ \Gamma^2 &= \sigma_3 \otimes \sigma_1 \otimes 1, \\ \Gamma^3 &= \sigma_3 \otimes \sigma_2 \otimes 1, \\ \Gamma^4 &= \sigma_1 \otimes 1 \otimes 1, \\ \Gamma^5 &= \sigma_2 \otimes 1 \otimes 1\end{aligned}\tag{A.18}$$

as a realization of the gamma matrices. As the matrix B satisfying (A.4), we can have

$$B = \Gamma^0\Gamma^1\Gamma^2\Gamma^4.\tag{A.19}$$

Since

$$\Gamma^0\Gamma^1\Gamma^2 = \sigma_3 \otimes \sigma_1 \otimes \sigma_3,\tag{A.20}$$

we can write B in a block form as

$$B = \begin{pmatrix} b & 0 \\ 0 & -b \end{pmatrix} \begin{pmatrix} 0 & \mathbf{1} \\ \mathbf{1} & 0 \end{pmatrix},\tag{A.21}$$

where

$$\sigma_1 \otimes \sigma_3 \equiv b.\tag{A.22}$$

$\mathbf{1}$ is the 4×4 unit matrix.

Since the chirality in six dimensions is defined by

$$\Gamma^\sharp \equiv -\Gamma^0\Gamma^1\Gamma^2\Gamma^3\Gamma^4\Gamma^5 \equiv (\sigma_3 \otimes \mathbf{1})(\mathbf{1} \otimes \gamma_5),\tag{A.23}$$

the eigenvalues of γ_5 and $(\sigma_3 \otimes \mathbf{1})$ are correlated with each other in a six-dimensional spinor with a definite chirality. For instance, if $\Gamma^\sharp = +1$, $(\gamma_5, \sigma_3) = (+, +)$ or $(-, -)$. Thus if we write

$$\psi_i = \begin{pmatrix} \phi_i \\ \chi_i \end{pmatrix} \quad (i = 1, 2), \quad (\text{A.24})$$

this is a decomposition with respect to the four-dimensional chirality. From (A.21), we have

$$\begin{aligned} \psi_i^c &= B\psi_i^* \\ &= \begin{pmatrix} b & 0 \\ 0 & -b \end{pmatrix} \begin{pmatrix} 0 & \mathbf{1} \\ \mathbf{1} & 0 \end{pmatrix} \begin{pmatrix} \phi_i^* \\ \chi_i^* \end{pmatrix} \\ &= \begin{pmatrix} b\chi_i^* \\ -b\phi_i^* \end{pmatrix}. \end{aligned} \quad (\text{A.25})$$

Therefore, if a collection of n spinors ψ_2 are written as ψ_1^c , the relations $\psi_2 = \psi_1^c$ and $\psi_1 = -\psi_2^c$ imply

$$\chi_2 = -b\phi_1^*, \quad \chi_1 = +b\phi_2^*. \quad (\text{A.26})$$

Thus the lower component of each of the $2n$ Weyl spinors can be expressed in terms of the upper component.

A.4 Restriction on the complex scalars

Let v_i ($i = 1, 2$) be a pair of n complex scalars and

$$\begin{pmatrix} v_1 \\ v_2 \end{pmatrix} \quad (\text{A.27})$$

be in the $\mathbf{2n}$ pseudo-real representation of G . In order to similarly define v_i^c such that

$$v_2 = v_1^c, \quad v_1 = -v_2^c \quad (\text{A.28})$$

by

$$v_i^c \equiv Uv_i^* \quad (\text{A.29})$$

for some U satisfying $U^*U = -1$, we recall that a hypermultiplet has *two* complex scalars transforming in the identical representation. Let $v_i^{(1)}$ and $v_i^{(2)}$ be such two scalars, then writing $v_i = \begin{pmatrix} v_i^{(1)} \\ v_i^{(2)} \end{pmatrix}$, we define

$$\begin{aligned} v_i^c &= \begin{pmatrix} v_i^{(1)c} \\ v_i^{(2)c} \end{pmatrix} \\ &\equiv U \begin{pmatrix} v_i^{(1)*} \\ v_i^{(2)*} \end{pmatrix}, \end{aligned} \quad (\text{A.30})$$

where

$$U \equiv \begin{pmatrix} 0 & -1 \\ 1 & 0 \end{pmatrix} \quad (\text{A.31})$$

is a $90^\circ U(1)_R$ rotation. Then $U^*U = -1$, and (A.28) can be imposed. With this definition of v_i^c , one can also reduce the degrees of freedom of the complex scalars in a hypermultiplet.

B Summary of $SU(6) \rightarrow E_6$

In this appendix we summarize the results of the analysis [11] of the codimension-two enhancement $SU(6) \rightarrow E_6$. Consider

$$\Phi = -y^2 + x^3 + (t_r^2 + 3t_r z)x^2 + (2t_r z^2 + 3z^3)x + z^4. \quad (\text{B.1})$$

One can verify that Φ has an $SU(6)$ singularity at (x, y, z) for fixed $t_r \neq 0$, and this is enhanced to an E_6 singularity for $t_r = 0$. Φ (B.1) can be obtained by putting $h_{n+2-r} = \frac{1}{\sqrt{3}}$, $H_{n+4-r} = -\frac{1}{2}$, $u_{r+4} = \frac{1}{2}$, $f_{n+8-r} = f_8 = g_{12} = 0$ in (2.8) and (2.9) and making a change of variables.

If we take $t_r = s$, we are led to the incomplete resolution. The process is summarized in Table 9. After the codimension-one blow up at the singularity p_0 of Φ (B.1), we obtain two exceptional curves $\mathcal{C}_{1\pm}$ at fixed $s \neq 0$, which come on top of each other into a single curve δ_1 at $s = 0$. These two curves intersect at a singularity p_1 , which forms a singular line along the s direction. We perform a codimension-one blow up along this line to find, again, two exceptional curves $\mathcal{C}_{2\pm}$ at $s \neq 0$, which becomes $\delta_{2\pm}$ at $s = 0$. The intersection of $\mathcal{C}_{2\pm}$ is again another singularity p_2 . We then blow up the singularity line p_2 to get a regular curve \mathcal{C}_3 at $s \neq 0$, which splits into two curves $\delta_{3\pm}$ at $s = 0$.

In the incomplete case, this is the end. The relations among \mathcal{C} 's and δ 's are given by

$$\begin{aligned} \mathcal{C}_{1\pm} &= \delta_1 + \delta_{3\pm}, \\ \mathcal{C}_{2\pm} &= \delta_{2\pm}, \\ \mathcal{C}_3 &= \delta_{3+} + \delta_{3-}. \end{aligned} \quad (\text{B.2})$$

One can derive these relations in the same way as explained in section 3.1.3. Their intersection diagrams are shown in Figure 15.

Table 9. $SU(6) \rightarrow E_6$: Incomplete case.

	1st blow up	2nd blow up	3rd blow up
$\mathcal{Q}_0 \rightarrow$	$\mathcal{Q}_1(0 : 0 : 1) \rightarrow$	$\mathcal{Q}_2(1 : 0 : -s) \rightarrow$	regular

For the complete resolution, we take $t_r = s^2$. In this case, as is shown in Table 10, we have an additional codimension-two isolated conifold singularity after the 3rd blow up.

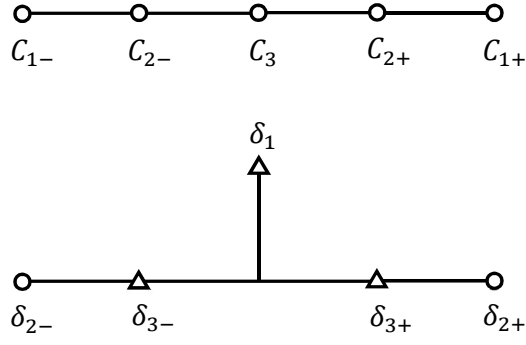


Figure 15. Generic intersection diagram at $s \neq 0$ (upper) and incomplete intersection diagram at $s = 0$ (lower) of $SU(6) \rightarrow E_6$.

The relations (B.2) are modified to

$$\begin{aligned}
 C_{1\pm} &= \delta_1 + \delta_{3\pm} + \delta_{\text{complete}}, \\
 C_{2\pm} &= \delta_{2\pm}, \\
 C_3 &= \delta_{3+} + \delta_{3-} + \delta_{\text{complete}}.
 \end{aligned}
 \tag{B.3}$$

This result is obtained by following the analysis explained in section 3.2.2. The intersection diagram of these six δ 's is the proper E_6 Dynkin diagram as in Figure 16.

Table 10. $SU(6) \rightarrow E_6$: Complete case.

	1st blow up	2nd blow up	3rd blow up	4th blow up
$\mathcal{P}_0 \rightarrow$	$\mathcal{P}_1(0 : 0 : 1) \rightarrow$	$\mathcal{P}_2(1 : 0 : -w) \rightarrow$	$\mathcal{P}_3(1 : 0 : 0; s = 0)(\text{codim.2}) \rightarrow$	regular

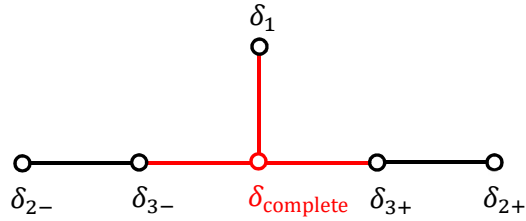


Figure 16. Complete E_6 intersection diagram of $SU(6) \rightarrow E_6$.

C Small resolution of a conifold singularity

In this appendix, we give a brief review of the small resolution (see, *e.g.*, [26]). A conifold \mathcal{M} is a three dimensional space given by the polynomial in \mathbb{C}^4

$$X_1X_4 - X_2X_3 = 0. \quad (\text{C.1})$$

It has a singularity at $(X_1, X_2, X_3, X_4) = (0, 0, 0, 0)$, which is called the conifold singularity. In general, an isolated singularity on a hypersurface in \mathbb{C}^4 can be resolved by inserting \mathbb{P}^3 in the ambient space \mathbb{C}^4 . For the conifold singularity, it is equivalent to inserting $\mathbb{P}^1 \times \mathbb{P}^1$ on the conifold \mathcal{M} . However, it is sufficient to insert only one \mathbb{P}^1 to resolve the conifold singularity. This process is called the small resolution. Inserting \mathbb{P}^1 at the origin of \mathcal{M} is given by

$$\check{\mathcal{M}} = \left\{ (X_1, X_2, X_3, X_4) \times (y_1 : y_2) \left| \begin{bmatrix} X_1 & X_2 \\ X_3 & X_4 \end{bmatrix} \begin{bmatrix} y_1 \\ y_2 \end{bmatrix} = \begin{bmatrix} 0 \\ 0 \end{bmatrix} \right. \right\}. \quad (\text{C.2})$$

Let us write $M = \begin{bmatrix} X_1 & X_2 \\ X_3 & X_4 \end{bmatrix}$. Since $(y_1 : y_2) \neq (0, 0)$, $\det M = 0$. This gives the defining equation of the conifold (C.1). Furthermore, if

$$(X_1, X_2, X_3, X_4) \begin{cases} \neq (0, 0, 0, 0) \Rightarrow \text{rank} M = 1 \Rightarrow (y_1 : y_2) \text{ is determined,} \\ = (0, 0, 0, 0) \Rightarrow \text{rank} M = 0 \Rightarrow (y_1 : y_2) \text{ is undetermined,} \end{cases}$$

which means that $\mathbb{P}^1 = (y_1 : y_2)$ is inserted only at the origin. As a result, $\check{\mathcal{M}}$ is regular, since $\partial_{X_1}(X_1y_1 + X_2y_2) = y_1 = 0$ and $\partial_{X_2}(X_1y_1 + X_2y_2) = y_2 = 0$ are not compatible.

$\check{\mathcal{M}}$ is covered by two local coordinate patches. If $y_1 \neq 0$, we can solve (C.2) as

$$X_1 = -\frac{y_2}{y_1}X_2, \quad X_3 = -\frac{y_2}{y_1}X_4, \quad (\text{C.3})$$

and hence

$$(X_1, X_2, X_3, X_4) = (-\lambda X_2, X_2, -\lambda X_4, X_4) \quad \text{with } \lambda \equiv \frac{y_2}{y_1}. \quad (\text{C.4})$$

We call this patch H_+ . Local coordinates of H_+ are (X_2, X_4, λ) and the inserted $\mathbb{P}^1 = (y_1 : y_2)$ is located at

$$(X_2, X_4, \lambda) = (0, 0, \lambda). \quad (\text{C.5})$$

If $y_2 \neq 0$, we can solve (C.2) as

$$X_2 = -\frac{y_1}{y_2}X_1, \quad X_4 = -\frac{y_1}{y_2}X_3, \quad (\text{C.6})$$

and hence

$$(X_1, X_2, X_3, X_4) = (X_1, -\mu X_1, X_3, -\mu X_3) \quad \text{with } \mu \equiv \frac{y_1}{y_2}. \quad (\text{C.7})$$

We call this patch H_- . Local coordinates of H_- are (X_1, X_3, μ) and the inserted \mathbb{P}^1 is

$$(X_1, X_3, \mu) = (0, 0, \mu). \quad (\text{C.8})$$

References

- [1] C. Vafa, Nucl. Phys. B **469**, 403 (1996) [hep-th/9602022].
- [2] E. Witten, Nucl. Phys. B **471** (1996) 135
- [3] R. Blumenhagen, B. Körs, D. Lüst, and T. Ott, Nucl. Phys. B **616**, 333 (2001) [hep-th/0107138].
- [4] R. Blumenhagen, M. Cvetič, D. Lüst, R. Richter, and T. Weigand, Phys. Rev. Lett. **100** (2008) 061602, 0707.1871.
- [5] D. R. Morrison and C. Vafa, Nucl. Phys. B **473**, 74 (1996) [hep-th/9602114].
- [6] D. R. Morrison and C. Vafa, Nucl. Phys. B **476**, 437 (1996) [hep-th/9603161].
- [7] M. Bershadsky, K. Intriligator, S. Kachru, D.R. Morrison, V. Sadov and C. Vafa, Nucl.Phys. B **481** (1996) 215-252 [hep-th/9605200].
- [8] S. H. Katz and C. Vafa, Nucl. Phys. B **497**, 146 (1997) [hep-th/9606086].
- [9] T. Tani, Nucl. Phys. B **602**, 434 (2001).
- [10] S. Mizoguchi, JHEP **1407**, 018 (2014) [arXiv:1403.7066 [hep-th]].
- [11] D. R. Morrison and W. Taylor, JHEP **1201**, 022 (2012) [arXiv:1106.3563 [hep-th]].
- [12] M. Gunaydin, G. Sierra and P. K. Townsend, Phys. Lett. B **133** (1983) 72.
- [13] M. Gunaydin, G. Sierra and P. K. Townsend, Nucl. Phys. B **242** (1984) 244.
- [14] H. Hayashi, C. Lawrie, D. R. Morrison and S. Schafer-Nameki, JHEP **1405**, 048 (2014) [arXiv:1402.2653 [hep-th]].
- [15] M. Esole and S. T. Yau, Adv. Theor. Math. Phys. **17**, no. 6, 1195 (2013) [arXiv:1107.0733 [hep-th]].
- [16] J. Marsano and S. Schafer-Nameki, JHEP **1111**, 098 (2011) [arXiv:1108.1794 [hep-th]].
- [17] M. Esole, S. H. Shao and S. T. Yau, Adv. Theor. Math. Phys. **19**, no. 6, 1183 (2015) [arXiv:1402.6331 [hep-th]]; Adv. Theor. Math. Phys. **20**, no. 4, 683 (2016) [arXiv:1407.1867 [hep-th]].
- [18] A. P. Braun and S. Schafer-Nameki, Nucl. Phys. B **905** (2016) 447 [arXiv:1407.3520 [hep-th]]; Nucl. Phys. B **905** (2016) 480 [arXiv:1511.01801 [hep-th]].
- [19] H. Pinkham, in Singularities (P. Orlik, ed.), vol. 40, part 2 of Proc. Symp. Pure Math., pp. 343-371, American Mathematical Society, 1983.
- [20] M. Reid, in Algebraic Varieties and Analytic Varieties (S. Iitaka, ed.), vol. 1 of Adv. Stud. Pure Math., pp. 131-180, Kinokuniya, 1983.
- [21] S. Katz and D. R. Morrison, J. Algebraic Geom. **1** (1992) 449-530, [arXiv:alg-geom/9202002].
- [22] R. Friedman, J. Morgan and E. Witten, Commun. Math. Phys. **187**, 679 (1997) [hep-th/9701162].
- [23] R. Donagi and M. Wijnholt, Adv. Theor. Math. Phys. **15**, 1237 (2011) [arXiv:0802.2969 [hep-th]].
- [24] S. Mizoguchi and T. Tani, JHEP **1611**, 053 (2016) [arXiv:1607.07280 [hep-th]].
- [25] K. Oguiso and T. Shioda, Comment. Math. Univ. St. Pauli. **40** (1991) 83.

- [26] P. Candelas and X. C. de la Ossa, Nucl. Phys. B **342** (1990) 246-268.
- [27] Y. Kimura, JHEP **1704**, 168 (2017) [arXiv:1608.07219 [hep-th]].
- [28] T. Kugo and T. Yanagida, Phys. Lett. **134B**, 313 (1984). doi:10.1016/0370-2693(84)90007-8
- [29] S. Mizoguchi and T. Tani, PTEP **2016**, no. 7, 073B05 (2016) [arXiv:1508.07423 [hep-th]].
- [30] J. J. Heckman, A. Tavanfar and C. Vafa, JHEP **1008**, 040 (2010) [arXiv:0906.0581 [hep-th]].
- [31] S. Fukuchi, N. Kan, S. Mizoguchi and H. Tashiro, Phys. Rev. D **100**, no. 12, 126025 (2019) [arXiv:1808.04135 [hep-th]].
- [32] S. Fukuchi, N. Kan, R. Kuramochi, S. Mizoguchi and H. Tashiro, Phys. Lett. B **803**, 135333 (2020) [arXiv:1912.02974 [hep-th]].